

# Targeting Kollo Skewness with Random Orthogonal Matrix Simulation

Carol Alexander\* Xiaochun Meng<sup>†</sup> Wei Wei<sup>‡</sup>

## Abstract

High-dimensional multivariate systems often lack closed-form solutions and are therefore resolved using simulation. Random Orthogonal Matrix (ROM) simulation is a state-of-the-art method that has gained popularity in this context because certain simulation errors are completely removed (Ledermann et al., 2011). Specifically, every sample generated with ROM simulation *exactly* matches a target mean and covariance matrix. A simple extension can also target a scalar measure of skewness or kurtosis. However, targeting non-scalar measures of higher moments is much more complex. [The problem of targetting exact Kollo skewness has already been considered, but the algorithm proceeds via time-consuming trial-and-error which can be very slow. Moreover, the algorithm often fails completely.](#) Furthermore, it produces simulations with very long periods of inactivity which are inappropriate for most real-world applications. This paper provides an in-depth theoretical analysis of a much quicker ROM simulation extension which always succeeds to target Kollo skewness exactly. [It also derives new results on Kollo skewness in concatenated samples and applies them](#) to produce realistic simulations for many applications, especially those in finance. Our first contribution is to establish necessary and sufficient conditions for Kollo skewness targeting to be possible. Then we introduce two novel methods, one for speeding up the algorithm and another for improving the statistical properties of the simulated data. We illustrate several new theoretical results with some extensive numerical analysis and we apply the algorithm using some real data drawn from two different multivariate systems of financial returns.

**Keywords:** Simulation; Algebraic statistics, L matrices, Multivariate skewness, ROM simulation

**JEL Codes:** C15, C63.

---

\*Corresponding author. University of Sussex Business School and Peking University PHBS Business School. Email: c.alexander@sussex.ac.uk

<sup>†</sup>University of Sussex Business School. Email: xiaochun.meng@sussex.ac.uk.

<sup>‡</sup>University of Sussex Business School. Email: wei.wei@sussex.ac.uk.

# 1 Introduction

Modelling multivariate systems is important for many applications in operational research but also in economics, engineering, environmental science, finance, medicine and other disciplines that require quantitative analysis. In the vast majority of cases, the multivariate distributions under scrutiny have no analytic or closed form, so the problem can only be resolved using some type of numerical technique. Of these, Monte Carlo (MC) simulation is most commonly used because it is fast, the basic method is quite straightforward and the random samples generated converge to the distribution in probability (Thomopoulos, 2012). However, the sample moments are not equal to their population values and even when the experimenter performs a very large number of simulations the differences can be considerable. As a result, sampling error and uncertainty in MC methods have been widely studied (see, for example, Oberkampf et al. 2002 and Ferraz and Moura 2012). For this reason, much research focusses on developing variance-reduction techniques aimed at improving the efficiency of simulations – see, for example, Swain and Schmeiser (1988), Hesterberg (1996), Szántai (2000), Saliby and Paul (2009) and many others. These have applications to any problem which requires the use of multivariate simulations for its resolution. For instance, see Badano and Samuelson (2013) and Quintana et al. (2015) for multivariate simulations used in engineering applications, and Avramidis and Matzinger (2002), Capriotti (2008), and Ma and He (2016) for problems in finance.

Addressing the simulation error problem from a different perspective entirely, Ledermann et al. (2011) introduces a novel and flexible method for generating random samples from a correlated, multivariate system called Random Orthogonal Matrix (ROM) simulation. It is based on the premise of *exactly* matching a target mean, covariance matrix and certain higher moments with *every* simulation. Several developments have extended the original paper, for instance, Ledermann and Alexander (2012) investigate the effect of different random rotation matrices on ROM simulation sample characteristics. And Hürlimann (2013) presents a very significant theoretical development of ROM simulation by extending the basic  $L$  matrices (which are fundamental to ROM simulation, as we shall see below) to a much broader class of generalised Helmert-Ledermann (GHL) matrices, thereby increasing flexibility and scope of ROM simulation.

ROM simulation has already been applied in a variety of real-world applications. For instance, Geyer et al. (2014) implements ROM simulation in an arbitrage-free setting, for option pricing and hedging. Hürlimann (2014) integrates ROM simulation into two semi-parametric methods that take into account skewness and kurtosis, in order to improve the computation of quantiles for linear combinations of the system variables, and Alexander and Ledermann (2012) investigate the use of target skewness and kurtosis via ROM simulation for stress testing. Further theoretical developments focus on the higher-moment characteristics of ROM simulation: Hürlimann (2015) introduces a new, recursive method for targeting the skewness and kurtosis metrics of Mardia (1970) using ROM simulation with GHL matrices, and Hanke et al. (2017) improve on the skewness metric that ROM simulation can target, using the vector-valued moment of Kollo (2008) in place of the Mardia skewness.

This paper extends the literature on higher-moment characteristics of ROM simulation by providing a new method for targeting Kollo skewness. The Hanke et al. (2017) algorithm requires

selecting a large number of so-called ‘arbitrary’ real values to determine a complex non-linear system of equations. However, the authors overlooked that these equations are often not solvable in the real numbers, an issue that becomes more and more prevalent as the dimension of the system increases.

Their algorithm entails a trial-and-error approach but we found that it never works in many cases, and when it does the simulations have long periods of zero or minimal activity interspersed with periods of high activity. This could be a useful feature for applications to climate modelling or medical research – for instance, such patterns are commonly observed in multivariate seismic wave dynamics (Takanami and Kitagawa 1991, Adelfio et al. 2012 and others) and cardiology (see McSharry et al. 2003, Lyon et al. 2018 and others). However, such extreme patterns have little relevance to problems in economics and finance.

We develop a novel ROM algorithm for targeting Kollo skewness, hereafter referred to as KROM, which utilizes a set of new, necessary and sufficient conditions for the existence of real solutions to the exact Kollo skewness equations. A numerical study demonstrates a very large reduction in computation time, and much lower failure rates [of finding arbitrary value compared with the trial-and-error approach in the existing algorithm](#). Being based on bootstrapping real data or parametric distributions KROM simulation offers the flexibility to generate simulations with statistical characteristics suitable to many applications of interest. It is ideally suited to modelling financial systems, which can be very high dimensional and have long been known to exhibit the type of conditional heteroscedasticity which arises naturally using the KROM algorithm.<sup>1</sup> An empirical study demonstrates its application to hourly cryptocurrency returns and daily returns on the sector indices of the S&P 500 index.

Another new theoretical result is used in KROM simulation to provide the option of sample concatenation. It is already known that concatenating samples generated by standard ROM simulation preserves the target mean and covariance matrix (Ledermann et al., 2011), but here we prove that sample concatenation can also leave Kollo skewness invariant, under certain conditions. Thus, concatenation may be applied to increase the scope of KROM simulation to reflect characteristics of real-world applications, especially in large systems. By contrast, the [existing](#) algorithm, when it works, produces simulations having strange dynamic properties and exceptionally high marginal kurtosis which limits the scope of its potential applications.

In the following: Section 2 fixes notation and concepts; Section 3 presents the new algorithm by deriving the necessary and sufficient conditions for real solutions of the Kollo skewness equations, proposing both non-parametric and parametric methods for generating simulations, presenting comprehensive numerical results which aim to guide the researcher to operate the algorithm by choosing appropriate parameters, and proving the invariance of Kollo skewness under sample concatenation; Section 4 reports our practical applications using real financial systems; and Section 5 summarises and concludes. All theoretical proofs and some further numerical results are given in the appendices and all Python and Matlab code is available from the authors on request.

---

<sup>1</sup>See Engle 1982, Bollerslev et al. 1994 and a highly-prolific theoretical and applied literature since then.

## 2 Background

In this section we fix notation by providing a brief overview of the basic concepts for both ROM simulation and multivariate skewness.

### 2.1 ROM Simulation

Suppose we want to simulate from an  $n$ -dimensional random variable with  $n \times 1$  mean vector  $\boldsymbol{\mu}_n$  and  $n \times n$  covariance matrix  $\mathbf{V}_n$ . Let  $\mathbf{X}_{mn}$  denote the  $m \times n$  matrix of simulations, where  $m$  denotes the number of observations. In order to match the mean and covariance of the samples  $\mathbf{X}_{mn}$  with  $\boldsymbol{\mu}_n$  and  $\mathbf{V}_n$ , the following equations must be satisfied:

$$m^{-1} \mathbf{1}'_m \mathbf{X}_{mn} = \boldsymbol{\mu}'_n, \quad (1)$$

$$m^{-1} \left( \mathbf{X}'_{mn} - \boldsymbol{\mu}_n \mathbf{1}'_m \right) \left( \mathbf{X}_{mn} - \mathbf{1}_m \boldsymbol{\mu}'_n \right) = \mathbf{V}_n, \quad (2)$$

where  $\mathbf{1}_m$  is a  $m \times 1$  column vector with all ones and  $'$  denotes the matrix transpose. Ledermann et al. (2011) show that (1) and (2) hold if and only if  $\mathbf{X}_{mn}$  takes the following form:

$$\mathbf{X}_{mn} = \mathbf{1}_m \boldsymbol{\mu}'_n + m^{1/2} \mathbf{Q}_m \mathbf{L}_{mn} \mathbf{R}_n \mathbf{A}_n, \quad (3)$$

$$\mathbf{L}'_{mn} \mathbf{L}_{mn} = \mathbf{I}_n, \quad (4)$$

$$\mathbf{1}'_m \mathbf{L}_{mn} = \mathbf{0}'_n, \quad (5)$$

where the  $n \times n$  matrix  $\mathbf{A}_n$  is derived using  $\mathbf{V}_n = \mathbf{A}'_n \mathbf{A}_n$ ,  $\mathbf{0}_n$  is the  $n \times 1$  vector with all zeros,  $\mathbf{I}_n$  is the  $n \times n$  identity matrix, and both  $\mathbf{Q}_m$  and  $\mathbf{R}_n$  are orthogonal matrices. In ROM simulation,  $\mathbf{Q}_m$  is a  $m \times m$  random permutation matrix which functions to re-order the observations;  $\mathbf{R}_n$  is a  $n \times n$  random rotation matrix which can re-generate  $\mathbf{X}_{mn}$  by simply changing  $\mathbf{R}_n$ , and the matrix  $\mathbf{L}_{mn}$  is taken from a class of rectangular  $m \times n$  orthogonal matrices known as  $L$  matrices. In equation (3), the sample mean and covariance of  $\mathbf{X}_{mn}$  are determined solely by  $\boldsymbol{\mu}_n$  and  $\mathbf{A}_n$ , given that  $\mathbf{L}_{mn}$  satisfies equations (4) and (5). Hence,  $L$  matrices are a cornerstone of ROM simulation and to generate  $\mathbf{X}_{mn}$  we must first obtain an  $L$  matrix.

In addition to the ability to match the exact mean and covariance matrix, ROM simulation is generally much faster than MC simulation, especially in high-dimensional systems, because samples are generated by simply changing  $\mathbf{R}_n$  to another random rotation matrix and performing the required matrix multiplications. See Ledermann and Alexander (2012) for the classification of different types of rotation matrix and their effects on ROM simulation sample characteristics.

### 2.2 Kollo Skewness

Consider a correlated system of  $n$  random variables  $\mathbf{Y}_n = [Y_1, Y_2, \dots, Y_n]$  having mean  $\boldsymbol{\mu}_n$  and covariance matrix  $\mathbf{V}_n$  and use the notation  $\mathbf{Y}_n^*$  for the standardised versions of  $\mathbf{Y}_n$ , i.e.

$$\mathbf{Y}_n^* = (\mathbf{Y}_n - \mathbf{1}_m \boldsymbol{\mu}'_n) \mathbf{V}_n^{-1/2}.$$

A typical way to define the skewness of their multivariate distribution is to set  $c_{ijk} = \mathbb{E}[Y_i^* Y_j^* Y_k^*]$  for each tuple  $(Y_i^*, Y_j^*, Y_k^*)$ , with  $i, j, k = 1, \dots, n$ . Then, for each  $i = 1, \dots, n$ , form the matrix

$$\mathbf{C}_i = \begin{bmatrix} c_{i11} & c_{i12} & \cdots & c_{i1n} \\ \vdots & \vdots & \ddots & \vdots \\ c_{in1} & c_{in2} & \cdots & c_{inn} \end{bmatrix},$$

and finally define the co-skewness tensor as:

$$\mathbf{m}_3 = [\mathbf{C}_1, \mathbf{C}_2, \dots, \mathbf{C}_n]. \quad (6)$$

This tensor has good properties such as invariance under affine, non-singular transformations (Mardia, 1970). However, it has  $n^3$  elements which makes it impractical for use in large systems, hence the need to construct summary skewness metrics.

Mardia (1970) proposes multivariate skewness as follows:

$$\beta_1(\mathbf{Y}_n) = \sum_{i,j,k=1}^n c_{ijk}^2. \quad (7)$$

It can be shown that Mardia skewness is essentially the sum of all the squared elements in (6). However, Gutjahr et al. (1999) show that, being a simple scalar, the Mardia skewness loses much of the information contained in the co-skewness tensor (6). To retain more information yet still employ a skewness measure that is more practical than the full co-skewness tensor, we shall focus on the  $n$ -dimensional skewness measure proposed by Kollo (2008) which is defined as:

$$\boldsymbol{\tau}(\mathbf{Y}_n) = \left[ \sum_{i,k}^n c_{i1k}, \sum_{i,k}^n c_{i2k}, \dots, \sum_{i,k}^n c_{ink} \right]'. \quad (8)$$

That is, the  $i^{\text{th}}$  element of the Kollo skewness vector is equal to the sum of the elements of the  $i$ -th row of  $\mathbf{m}_3$ . It takes information from all elements of the co-skewness tensor, whereas the other multivariate skewness measures proposed by Móri et al. (1994) and Balakrishnan et al. (2007) omit third-order mixed moments. Because of this, Kollo skewness performs better for asymmetric multivariate distributions, as demonstrated by Jammalamadaka et al. (2020).

### 2.3 The Algorithm of Hanke et al. (2017)

Let  $\boldsymbol{\mu}_n$ ,  $\mathbf{V}_n$  and  $\boldsymbol{\tau}_n$  be the target mean vector, covariance matrix, and Kollo skewness vector that we want to match. Equations (3) – (5) only guarantee that  $\mathbf{X}_{mn}$  matches the target mean and covariance, but it remains to match Kollo skewness which can be affected by  $\mathbf{L}_{mn}$  and  $\mathbf{R}_n$ . We seek a suitable  $m^{-1/2} \mathbf{L}_{mn} \mathbf{R}_n$ , a standardised version of  $\mathbf{X}_{mn}$ , which also satisfies equation (8).

For convenience, we now re-state the Hanke et al. (2017) algorithm in a different form because this clarifies the solvability issues that we wish to focus on. To this end, define the scaled  $L$  matrix  $m^{1/2} \mathbf{L}_{mn} \mathbf{R}_{mn} = \mathbf{M}_{mn} = \mathbf{S}_{mn} \boldsymbol{\Omega}'_n$  where  $\mathbf{S}_{mn}$  is also a scaled  $L$  matrix and  $\boldsymbol{\Omega}_n$  is any orthogonal

rotation matrix whose first column is  $n^{-1/2}\mathbf{1}_n$  having the property that:

$$\mathbf{1}'_n \boldsymbol{\Omega}_n = n^{1/2} [1, 0, \dots, 0]. \quad (9)$$

As a consequence, the algorithm aims to find  $\mathbf{S}_{mn}$  and then obtain  $\mathbf{X}_{mn}$  using:

$$\mathbf{X}_{mn} = \mathbf{1}_m \boldsymbol{\mu}'_n + \mathbf{Q}_m \mathbf{S}_{mn} \boldsymbol{\Omega}'_n \mathbf{A}_n. \quad (10)$$

According to the definition, to solve the equations  $\boldsymbol{\tau}(\mathbf{X}_{mn}) = \boldsymbol{\tau}_n$  for some target Kollo skewness vector  $\boldsymbol{\tau}_n$  the scaled  $L$  matrix should satisfy:

$$\boldsymbol{\tau}_n = m^{-1} \sum_{i=1}^m (\mathbf{r}_i \mathbf{1}_n)^2 \mathbf{r}'_i = m^{-1} \sum_{i=1}^m (\mathbf{s}_i \boldsymbol{\Omega}'_n \mathbf{1}_n)^2 \boldsymbol{\Omega}_n \mathbf{s}'_i = m^{-1} n \boldsymbol{\Omega}_n \sum_{i=1}^m s_{i1}^2 \mathbf{s}'_i. \quad (11)$$

where  $\mathbf{r}_i$  is the  $i$ -th row of  $\mathbf{M}_{mn}$  and  $\mathbf{s}_i$  is the  $i$ -th row of  $\mathbf{S}_{mn}$ ,  $i = 1, \dots, m$ . Pre-multiplying the matrix  $n^{-1} \boldsymbol{\Omega}'_n$  on both sides of equation (11) the system may now be written:

$$\mathbf{p}_n = m^{-1} \sum_{i=1}^m s_{i1}^2 \mathbf{s}'_i, \quad (\text{Exact Kollo skewness}) \quad (12)$$

where the rotated Kollo skewness vector  $\mathbf{p}_n = n^{-1} \boldsymbol{\Omega}'_n \boldsymbol{\tau}_n$ . In addition, because  $\mathbf{S}_{mn}$  is a scaled  $L$  matrix, it must satisfy:

$$\mathbf{S}'_{mn} \mathbf{S}_{mn} = m \mathbf{I}_n, \quad (\text{Exact covariance matrix}) \quad (13)$$

$$\mathbf{1}'_m \mathbf{S}_{mn} = \mathbf{0}'_n. \quad (\text{Column sum constraint}) \quad (14)$$

The above formulation of the exact Kollo skewness equations highlights three necessary and sufficient conditions (12) – (14) for  $\mathbf{S}_{mn}$  to realise a ROM simulation with target moments  $\boldsymbol{\mu}_n$ ,  $\mathbf{V}_n$  and  $\boldsymbol{\tau}_n$  via equation (10). However, this formulation does not identify how these equations can be solved. To this end, let  $s_{1k}, \dots, s_{mk}$  denote the elements in the  $k$ -th column of  $\mathbf{S}_{mn}$  and  $p_k$  denote the  $k$ -th element of  $\mathbf{p}_n$ . Note that our theoretical results in the next section will highlight the importance of the first element of  $\mathbf{p}_n$  given by  $p_1 = n^{-3/2} \mathbf{1}'_n \boldsymbol{\tau}_n$ . With this notation, for each column  $k$ , we have an alternative expression for equations (12) – (14) as follows:

$$m^{-1} \sum_{i=1}^m (s_{i1})^2 s_{ik} = p_k, \quad (\text{Exact Kollo skewness}) \quad (15-1)$$

$$m^{-1} \sum_{i=1}^m s_{ik}^2 = 1, \quad (\text{Exact covariance matrix 1}) \quad (15-2)$$

$$\sum_{i=1}^m s_{ik} s_{ij} = 0, \quad j < k, \quad (\text{Exact covariance matrix 2}) \quad (15-3)$$

$$\sum_{i=1}^m s_{ik} = 0. \quad (\text{Column sum constraint}) \quad (15-4)$$

We need to solve equations (15-1) to (15-4) sequentially, from  $k = 1$  to  $k = n$ . However, there are  $m$  unknown variables in each column but there are only  $k + 2$  constraints in the  $k^{\text{th}}$  column. For example, for  $k = 1$  the  $m$  unknowns are  $s_{11}, s_{21}, \dots, s_{m1}$ , but there are only 3 constraints. [Prescribing arbitrary values  \$w\_{ik}\$  to some of the unknowns can address this under-determinacy problem.](#) Specifically, the last  $m - (k + 2)$  elements in each column  $k$  are set to arbitrary values, i.e.  $s_{ik} = w_{ik}$  for  $i = k + 3, \dots, m$  and for  $k = 1, \dots, n$ . In the code supplied they set  $w_{i1} = 0$  for  $i = 4, \dots, m$ , and for  $k = 2, \dots, n$  they draw  $w_{ik}$  randomly from a uniform distribution on  $[0, 1]$ . This construction forces the exact Kollo skewness structure to be derived entirely from the first few elements in each column of  $\mathbf{S}_{mn}$ . That is, the vast majority of elements in each simulation have no effect on the value of Kollo skewness.

Another problem arises from the following statement in Hanke et al. (2017): “In this procedure, arbitrary values can be prescribed on several occasions. By varying these values, e.g. by setting them as random values, different  $L$  matrices can be constructed, all of which exactly match the pre-specified Kollo skewness vector.” However, equations (15-1) to (15-4) cannot always be solved. That is, their so-called ‘arbitrary’ values are not always admissible for this system of non-linear equations to have solutions in the real numbers. This may be seen immediately, for example, by rewriting equation (15-2) as

$$s_{1k}^2 + \dots + s_{k+2,k}^2 = m - \sum_{i=k+3}^m w_{ik}^2,$$

which must clearly have complex roots when the arbitrary values  $w_{ij}$  are such that  $\sum_{i=j+3}^m w_{ij}^2 > m$ .

Yet another complication arises because the additional restriction that each simulation has exact Kollo skewness dramatically increases the complexity of the computations, so it is very much slower than the original ROM simulation algorithm of Ledermann et al. (2011). For clarity, we summarise the main weaknesses of the algorithm as follows:

1. The statistical characteristics of the samples generated by the algorithm are unsuited to many applications because the vast majority of elements in the simulation are arbitrary values that are either zero or have minimal variation;
2. There is no guarantee that the algorithm works, and when it does work it can be very slow, which further reduces its appeal for practical implementation.

### 3 A New ROM Algorithm to Target Kollo Skewness

On closer inspection an algorithm that targets Kollo skewness could be made very much faster if we could find a way to minimize the number of trials taken to produce a set of arbitrary values for which (15-1) to (15-4) actually has real solutions. This motivates our first theoretical result, Theorem 1 in Section 3.1, which proves the necessary and sufficient conditions for the arbitrary values to be admissible, thereby circumventing weakness (2) above. Then, to overcome weakness (1) as well, Section 3.2 proposes a new ROM simulation algorithm with target Kollo skewness, or

KROM simulation for short, which utilizes Theorem 1 in the context of a statistical bootstrap or a parametric distribution. We also establish a practically useful theoretical result that allows the option to use sample concatenation in KROM simulation, i.e. to join several small sub-samples into one simulation. Finally, Section 3.3 presents some numerical results on the computational speed of our algorithm, demonstrates how failure rates vary with both system and sample sizes, and with the variance of the arbitrary values used to solve the Kollo skewness equations, and finally exhibits the effect of using the concatenation option.

### 3.1 Solving the Kollo Skewness Equations

Suppose that the last  $m - (k + 2)$  elements in each column  $k$  are set to arbitrary values and consider the necessary and sufficient conditions for these arbitrary values to be admissible. Equations (15-1) to (15-4) must be solved iteratively, for  $j = 1, 2, \dots, n$ . First consider the case  $j = 1$ . Setting  $s_{ij} = w_{ij}$  for  $i = 4, \dots, m$  we can simplify and rewrite the system (15-1) to (15-4) as the following three equations:

$$s_{11} + s_{21} + s_{31} = - \sum_{i=4}^m w_{i1} =: a \quad (16-1)$$

$$s_{11}^2 + s_{21}^2 + s_{31}^2 = m - \sum_{i=4}^m w_{i1}^2 =: b \quad (16-2)$$

$$s_{11}^3 + s_{21}^3 + s_{31}^3 = mp_1 - \sum_{i=4}^m w_{i1}^3 =: c. \quad (16-3)$$

**Lemma 1.** *A necessary and sufficient condition for the system (16-1) to (16-3) to have real solutions for  $s_{11}, s_{21}$  and  $s_{31}$  is:*

$$\left(b - \frac{a^2}{3}\right)^3 \geq 6 \left(c - ab + \frac{9}{2}a^3\right)^2. \quad (17)$$

The proof is in Appendix A. Now consider the case when  $j = 2, \dots, n$ . The system (15-1) to (15-4) is solved iteratively, so we assume it is solvable in the real numbers for  $j = 1, \dots, k - 1$ , and then seek necessary and sufficient conditions for the system to be solvable when  $j = k$ . In this case, the system (15-1) to (15-4) is most succinctly expressed in matrix form, as:

$$\mathbf{U}\mathbf{y} = \mathbf{v}, \quad (18)$$

$$\mathbf{y}'\mathbf{y} = m - \sum_{i=k+3}^m w_{ik}^2. \quad (19)$$

where  $\mathbf{y}$  is a column vector containing all the variables we want to solve, i.e.  $(s_{1,k}, \dots, s_{k+2,k})'$  and



$$\mathbf{U} = \begin{bmatrix} s_{11}^2 & s_{21}^2 & \cdots & s_{k+2,1}^2 \\ s_{11} & s_{21} & \cdots & s_{k+2,1} \\ s_{12} & s_{22} & \cdots & s_{k+2,2} \\ \vdots & \vdots & \vdots & \vdots \\ s_{1,k-1} & s_{2,k-1} & \cdots & s_{k+2,k-1} \\ 1 & 1 & 1 & 1 \end{bmatrix}, \mathbf{v} = \begin{bmatrix} mp_k - \sum_{i=k+3}^m s_{i1}^2 w_{ik} \\ - \sum_{i=k+3}^m s_{i1} w_{ik} \\ - \sum_{i=k+3}^m s_{i2} w_{ik} \\ \cdots \\ - \sum_{i=k+3}^m s_{i,k-1} w_{ik} \\ - \sum_{i=k+3}^m w_{ik} \end{bmatrix}.$$

Thus  $\mathbf{U}$  is a  $(k+1) \times (k+2)$  coefficient matrix and  $\mathbf{v}$  is a column vector. In practical applications we have always found that the column span of  $\mathbf{U}$  equals  $k+1$ , i.e. the matrix is full row rank. However, in some applications it could be that they are not. So, let  $\mathbf{U}_1$  be a matrix containing all the linearly independent columns of  $\mathbf{U}$ , with the remaining columns in the matrix  $\mathbf{U}_2$ . Denote by  $\mathbf{U}_1^+$  the Moore-Penrose inverse of  $\mathbf{U}_1$  which is defined as  $\mathbf{U}_1^+ = (\mathbf{U}_1' \mathbf{U}_1)^{-1} \mathbf{U}_1'$ .

**Theorem 1.** *A real solution of (15-1) – (15-4) exists iff the following three conditions hold:*

- (i) *The arbitrary values selected in the first column of  $\mathbf{S}_{mn}$  satisfy (16-1) – (16-3) and (17);*
- (ii) *When admissible values exist for columns 1 to  $k-1$  then the arbitrary values in the  $k$ -th column ( $k = 2, \dots, n$ ) of  $\mathbf{S}_{mn}$  have  $\text{Rank}(\mathbf{U}) = \text{Rank}([\mathbf{U}, \mathbf{v}])$  where  $[\mathbf{U}, \mathbf{v}]$  is the augmented matrix;*
- (iii) *The arbitrary values selected in the  $k$ -th column ( $k = 2, \dots, n$ ) of  $\mathbf{S}_{mn}$  also have*

$$\mathbf{g}' \mathbf{G}^{-1} \mathbf{g} - \mathbf{v}' (\mathbf{U}_1 \mathbf{U}_1')^+ \mathbf{v} \geq \sum_{j=i+3}^m w_{ji}^2 - m$$

where

$$\mathbf{G} = \mathbf{I} + \mathbf{U}_2' (\mathbf{U}_1 \mathbf{U}_1')^+ \mathbf{U}_2 \quad \text{and} \quad \mathbf{g} = \mathbf{U}_2' (\mathbf{U}_1 \mathbf{U}_1')^+ \mathbf{v}.$$

Although complex theoretically, this result is easy to code. It improves on the computational efficiency substantially, because the three conditions are easy to check. Without this result one must run a complex, large dimensional non-linear optimization algorithm numerous times, to search by trial-and-error for real roots of a very large number of equations, which may not even exist. So, if the algorithm works, it is rather slow.

Recall that one weakness of the Hanke et al. (2017) algorithm is that zero arbitrary values produce simulations with very long periods with no activity, and this seriously limits their practical applications. Yet another problem with zero arbitrary values is that they are not always admissible, so the algorithm may not work. To see this, we derive a simple corollary to Theorem 1 which is proved in Appendix A:

**Corollary 1.** *Zero arbitrary values  $w_{ik} = 0$  are admissible if and only if*

$$p_1^2 \leq \frac{m}{6} \quad \text{and} \quad p_k^2 \leq \frac{t}{m} + \frac{m}{(k+1)(k+1)} \quad \forall k > 1,$$

where  $t = s_{11}^4 + s_{21}^4 + s_{31}^4 - m \left( \frac{m}{k+1} + p_1^2 + \cdots + p_{k-1}^2 \right) > 0$

Hence, the algorithm is more likely to fail with zero arbitrary values when an element  $p_k$  of the rotated Kollo skewness is large and the sample size  $m$  is small.

### 3.2 The KROM Algorithm

The conditions of Corollary 1 are less strict than the conditions of Theorem 1 with non-zero arbitrary values. However, we do not advise using zero values in practice, because then it is not only the Kollo skewness, but also the mean and covariance, that are derived entirely from the first  $k + 2$  elements in the  $k$ -th column, for  $k = 1, \dots, n$ . This can cause impractical distortions in the simulations, such as excessively high kurtosis and long periods of inactivity. Clearly, we need to be more careful about solving the indeterminate system of Kollo skews equations, so here we propose two novel approaches: using a statistical bootstrap, and using parametric distributions.

Suppose the target moments are derived from a sample  $\mathbf{X}_{ln}^*$  where  $l$  is the number of observations and  $n$  is the number of variables – we distinguish this from  $\mathbf{X}_{mn}$  i.e. the samples generated using ROM simulation. We derive the corresponding scaled  $L$  matrix using a rotation matrix  $\mathbf{\Omega}_n$  as:

$$\mathbf{S}_{ln}^* = \left( \mathbf{X}_{ln}^* - \mathbf{1}_l \boldsymbol{\mu}'_n \right) \mathbf{A}_n^{-1} \mathbf{\Omega}_n. \quad (20)$$

For each column  $k$  we bootstrap  $m - (k + 2)$  values from the corresponding column of  $\mathbf{S}_{ln}^*$  and we denote these bootstrapped values  $z_{ik}$ ,  $i = k + 3, \dots, m$ . Note that this does not impose any restriction on the dependency between columns, so we can simply do this bootstrap independently, column by column. This is the simplest approach but it seems desirable anyway because the columns of  $\mathbf{S}_{mn}$  should have zero correlation.

Based on these values, the next task is to solve equations (15-1) to (15-4) to obtain columns with exactly zero mean, unit standard deviation and zero pair-wise correlation – as well as exact Kollo skewness. For each bootstrapped sample we need to verify a solution to the simultaneous equations (15-1) to (15-4). Now, since each column of  $\mathbf{S}_{ln}^*$  has zero mean and unit standard deviation, it may well be that  $\sum_{i=k+3}^m z_{ik}^2 \geq m$  and in this case equation (15-2) has no real roots. Therefore, we set

$$\bar{z} = \frac{1}{m - (k + 2)} \sum_{i=k+3}^m z_{ik} \quad \text{and} \quad s_z^2 = \frac{1}{m - (k + 2)} \sum_{i=k+3}^m (z_{ik} - \bar{z})^2,$$

and transform the bootstrapped values  $z_{ik}$  to  $w_{ik}$  given by:

$$w_{ik} = \sigma \left( \frac{z_{ik} - \bar{z}}{s_z} \right), \quad i = k + 3, \dots, m. \quad (21)$$

Now,  $\sigma \in (0, 1)$  is set by the user to ensure that  $\sum_{i=k+3}^m z_{ik}^2 < m$ . Lower values of  $\sigma$  are more likely to result in real roots for (15-2) although no positive target value of  $\sigma$  is guaranteed to work. There is a trade off between setting a high  $\sigma$  to maximize sampling variation in the bootstrap and a low  $\sigma$  which reduces the failure rate. We still need to solve the whole system (15-1) to (15-4) and by virtue of simulation there will always be some values for which there is no solution. See Section 4 for an analysis of various judicious values for  $\sigma$  in an empirical application of failure rates.

As an alternative to bootstrapping we may select the values from some representative parametric distributions, such as may be required in financial applications like risk management and portfolio optimization. This way, we combine univariate MC simulation with solving equations (15-1) to (15-4). As with the bootstrap, we may draw columns independently from any set of univariate marginal distributions which – if we wish to exploit the maximum distributional flexibility of ROM simulation – can be chosen to have very different statistical properties. Nevertheless, when we do an empirical comparison of failure rates in Section 4 we shall only consider values that are drawn from the same distribution family for each marginal.

Sample concatenation refers to the idea of “stitching” a finite number of samples to form a larger sample. In mathematical notation, let  $\mathbf{M}^{(k)}$ ,  $k = 1, 2, \dots, N$  be  $N$  sample matrices, each with dimension  $m_k \times n$ , then the sample concatenation of  $\mathbf{M}^{(k)}$  leads to a larger sample  $[\mathbf{M}^{(1)'}, \dots, \mathbf{M}^{(N)'}]'$ . Ledermann et al. (2011) first apply the sample concatenation method in ROM simulation. They show that the mean and covariance matrix of the concatenated samples are preserved if each constituent has identical mean and covariance matrix. Our next theoretical result shows how to ensure that Kollo skewness is also preserved under sample concatenation:

**Theorem 2.** *Let  $\mathbf{M}^{(k)}$  be a scaled  $L$  matrix of dimension  $m_k \times n$  with  $m_k \geq n + 2$ . Denote the  $i^{\text{th}}$  row of  $\mathbf{M}^{(k)}$  by  $\mathbf{r}_i^{(k)}$ , for  $i = 1, \dots, N$  where  $N$  is the number of concatenations. Then the Kollo skewness of the concatenated sample is the weighted sum of their Kollo skewnesses, i.e.*

$$\begin{aligned} \tau \left( \begin{bmatrix} \mathbf{M}^{(1)} \\ \vdots \\ \mathbf{M}^{(N)} \end{bmatrix} \right) &= \frac{1}{m_1 + \dots + m_N} \left( \sum_{i=1}^{m_1} \left( \mathbf{r}_i^{(1)} \mathbf{1}_n \right)^2 \mathbf{r}_i^{(1)'} + \dots + \sum_{i=1}^{m_N} \left( \mathbf{r}_i^{(N)} \mathbf{1}_n \right)^2 \mathbf{r}_i^{(N)'} \right) \\ &= \frac{1}{m_1 + \dots + m_N} \left( m_1 \tau \left( \mathbf{M}^{(1)} \right) + \dots + m_N \tau \left( \mathbf{M}^{(N)} \right) \right), \end{aligned} \quad (22)$$

It follows from Theorem 2 that Kollo skewness is invariant under sample concatenation, provided it is achieved via a set of (scaled)  $L$  matrices having identical dimensions and the same Kollo skewness.

KROM simulation requires the rotation matrix  $\mathbf{\Omega}_n$  to satisfy equation (9). This is the one we use for the numerical results in Section 3.3:

$$\begin{pmatrix} \frac{1}{\sqrt{n}} & \frac{(-1)^{n-1}}{\sqrt{n/(n-1)}} & 0 & 0 & \dots & 0 & 0 & 0 \\ \frac{1}{\sqrt{n}} & \frac{(-1)^n}{\sqrt{n(n-1)}} & \frac{(-1)^{n-1}}{\sqrt{(n-1)/(n-2)}} & 0 & \dots & 0 & 0 & 0 \\ \frac{1}{\sqrt{n}} & \frac{(-1)^n}{\sqrt{n(n-1)}} & \frac{(-1)^n}{\sqrt{(n-1)(n-2)}} & \frac{(-1)^{n-1}}{\sqrt{(n-2)/(n-3)}} & \dots & 0 & 0 & 0 \\ \frac{1}{\sqrt{n}} & \frac{(-1)^n}{\sqrt{n(n-1)}} & \frac{(-1)^n}{\sqrt{(n-1)(n-2)}} & \frac{(-1)^n}{\sqrt{(n-2)(n-3)}} & \dots & 0 & 0 & 0 \\ \vdots & \vdots & \vdots & \vdots & \vdots & \vdots & \vdots & \vdots \\ \frac{1}{\sqrt{n}} & \frac{(-1)^n}{\sqrt{n(n-1)}} & \frac{(-1)^n}{\sqrt{(n-1)(n-2)}} & \frac{(-1)^n}{\sqrt{(n-2)(n-3)}} & \dots & \frac{(-1)^n}{\sqrt{4 \times 3}} & \frac{(-1)^{n-1}}{\sqrt{3/2}} & 0 \\ \frac{1}{\sqrt{n}} & \frac{(-1)^n}{\sqrt{n(n-1)}} & \frac{(-1)^n}{\sqrt{(n-1)(n-2)}} & \frac{(-1)^n}{\sqrt{(n-2)(n-3)}} & \dots & \frac{(-1)^n}{\sqrt{4 \times 3}} & \frac{(-1)^n}{\sqrt{3 \times 2}} & \frac{(-1)^{n-1}}{\sqrt{2}} \\ \frac{1}{\sqrt{n}} & \frac{(-1)^n}{\sqrt{n(n-1)}} & \frac{(-1)^n}{\sqrt{(n-1)(n-2)}} & \frac{(-1)^n}{\sqrt{(n-2)(n-3)}} & \dots & \frac{(-1)^n}{\sqrt{4 \times 3}} & \frac{(-1)^n}{\sqrt{3 \times 2}} & \frac{(-1)^n}{\sqrt{2}} \end{pmatrix}.$$

We may now summarize the general KROM algorithm, with the option of sample concatenation, in the following pseudo-code:

---

**Algorithm 1** KROM algorithm

---

The main code, with subsample concatenation option:

```

1: function KROM( $m, \boldsymbol{\mu}, \mathbf{V}, \boldsymbol{\tau}, N$ )                                ▷  $m$ : sample size,  $\boldsymbol{\mu}, \mathbf{V}, \boldsymbol{\tau}$ : target moments,  $N$ : subsample size
2:    $l = \max \{n + 2, \lfloor \frac{m}{N} \rfloor\}$                                        ▷  $\lfloor x \rfloor$  returns the greatest integer less than or equal to  $x$ 
                                                                                   ▷ obtain the first  $N - 1$  subsamples with length  $l$ 

3:   for  $k = 1, \dots, N - 1$  do
4:      $\mathbf{M}_{(kl-k+1):kl, n} = \text{KROM\_GETM}(l, \boldsymbol{\tau})$ 
                                                                                   ▷ obtain the last sub-samples with length  $m - l(N - 1)$ 

5:    $\mathbf{M}_{(Nl-l+1):m, n} = \text{GETM}(m - Nl - l, \boldsymbol{\tau})$ 
6:   obtain  $\mathbf{A}_n$                                                                                                        ▷  $\mathbf{A}'\mathbf{A} = \mathbf{V}$ 
7:   generate  $\mathbf{Q}_m$                                                                                                    ▷  $\mathbf{Q}_m$  is a  $m \times m$  random permutation matrix
8:    $\mathbf{X}_{mn} = \mathbf{1}_m \boldsymbol{\mu} + \mathbf{Q}_m \mathbf{M} \mathbf{A}_n$                                        ▷ rotate back to get simulation  $\mathbf{X}_{mn}$ 
9:   return  $\mathbf{X}_{mn}$ 

```

A function to generate the matrix:  $\mathbf{M}_{mn}$

```

1: function GETM( $m, \boldsymbol{\tau}$ )                                                    ▷  $m$ : the number of observations,  $\boldsymbol{\tau}$ : target Kollo skewness
2:    $n = \text{length}(\boldsymbol{\tau})$ 
3:   generate  $\boldsymbol{\Omega}_n$                                                                                                        ▷  $\boldsymbol{\Omega}_n$  is a  $n \times n$  rotation matrix satisfying equation (9)
4:    $\mathbf{p}_n = \boldsymbol{\Omega}_n^{-1} n^{-1} \boldsymbol{\tau}$                                                                                        ▷ obtain the rotated Kollo skewness
                                                                                   ▷ solve for the first column

5:   while Theorem 1 (i) does not hold do
6:     generate random values  $\{z_{41}, \dots, z_{m1}\}$  by bootstrapping or from a distribution
7:     obtain  $\{w_{41}, \dots, w_{m1}\}$  using (21) and check Theorem 1 (i)
8:     if Theorem 1 (i) holds then
9:       fill  $\{s_{41}, \dots, s_{m1}\}$  with  $\{w_{41}, \dots, w_{m1}\}$ 
10:    solve (15-1) to (15-4) for elements  $\{s_{11}, \dots, s_{31}\}$                 ▷ solve for rotated Kollo skewness column by column
11:    for  $k = 2, \dots, n$  do
12:      while Theorem 1(ii) and (iii) do not hold do
13:        generate random values  $\{z_{k+3k}, \dots, z_{mk}\}$  by bootstrapping or from a distribution
14:        obtain  $\{w_{k+3k}, \dots, w_{mk}\}$  using (21) and check Theorem 1 (ii) and (iii)
15:        if Theorem 1 (ii) and (iii) hold then
16:          fill  $\{s_{k+3k}, \dots, s_{mk}\}$  with  $\{w_{k+3k}, \dots, w_{mk}\}$ 
17:        solve (15-1) to (15-4) to obtain elements  $\{s_{1k}, \dots, s_{k+2k}\}$ 
18:     $\mathbf{M}_{mn} = \mathbf{S}_{mn} \boldsymbol{\Omega}_n'$                                                                                        ▷ rotate back to get  $\mathbf{M}_{mn}$ 
19:    return  $\mathbf{M}_{mn}$ 

```

---

To generate the matrix  $\mathbf{M}_{mn}$  one may select any parametric distribution, the choice is not constrained. However, when making this choice the researcher should bear two points in mind. First, the skewness that one can attain this way may be restricted, depending on the family selected. For instance, the skewness is zero when a Student's t distribution is used. In Appendix C we derive the attainable skewness (under zero mean and unit variance) for some other well-known distributions: the skew-normal, the normal inverse Gaussian and the beta distribution. Another point to note is that the choice of distribution may affect the failure rates of the algorithm because the Kollo skewness equations need not be solvable. For instance, an obvious candidate for the parametric distribution is a normal distribution but this is highly likely to fail unless the target Kollo skewness is the zero vector. We derive some additional theoretical results in Appendix B for this normal case, showing that the  $\sigma$  resulting in admissible values increases monotonically with any pre-specified failure rate  $\alpha$ . The proof, which is essentially based on the central limit theorem, is lengthy and

tedious. To prevent the theoretical treatment becoming too overwhelming, we do not discuss this result further in the main text, but refer readers to Appendix B.

### 3.3 Numerical Results

Next we provide a simulation study which demonstrates the computational efficiency gained using our proposed KROM algorithm and demonstrates the effect of the concatenation option. First, Table 1 compares the average computation time required to implement KROM simulations with those produced using the Hanke et al. (2017) algorithm. For each value of  $n$  and  $m$ , we randomly generate 100 target Kollo skewness vectors with each element chosen from the uniform distribution  $\mathcal{U}(-1, 1)$ . For each of these 100 target Kollo skewness vectors, we note the time required to implement the both algorithms, and we report the mean and standard deviation of these 100 values. From the column labelled ‘Improvement’ we see that the KROM algorithm is always faster, and can be more than 10 times faster, than the [trial-and-error method](#) .

Table 1: **Computational Speed Comparison.**

The simulations have  $m$  observations on  $n$  random variables with zero mean, identity covariance and a random target Kollo skewness vector with each element randomly chosen from  $\mathcal{U}(-1, 1)$ . Means and standard deviations (in brackets) of computation times are derived from 100 random vectors per pair  $(m, n)$  and the arbitrary values are from  $\mathcal{N}(0, 0.7)$ . The KROM algorithm is compared with the algorithm proposed by Hanke et al. (2017) (HPSW) using the improvement ratio of mean computation times. The machine used is an Intel Core i5-8250U CPU, 3.41 gigahertz, with 8 gigabyte RAM, running python under Windows.

$m$	$n = 5$			$n = 10$		
	HPSW	KROM	Improvement	HPSW	KROM	Improvement
$5n$	0.670 (0.424)	0.117 (0.056)	5.73	2.170 (1.326)	0.243 (0.091)	8.93
$10n$	1.007 (0.540)	0.099 (0.040)	10.17	2.280 (0.788)	0.262 (0.112)	8.70
$20n$	1.425 (0.465)	0.163 (0.107)	8.84	2.747 (2.032)	0.409 (0.125)	6.72
$50n$	2.788 (3.340)	0.279 (0.156)	9.99	3.670 (4.691)	0.710 (0.200)	5.17
$100n$	3.792 (3.238)	0.384 (0.165)	9.88	15.288 (14.720)	6.529 (9.898)	2.34

The conditions derived in Theorem 1 for the Kollo skewness equations to be solvable in the real numbers depend on the target Kollo skewness  $\tau_n$ , the system dimension  $n$  and the simulation sample size  $m$ . There is no guarantee and it may be that, for certain values of these parameters, all bootstraps or draws from a parametric distribution are inadmissible, i.e. there is no real solution to (15-1) – (15-4). Then, the KROM algorithm fails because the user has specified parameters that are inconsistent with a solution. How does the failure rate of KROM simulation algorithm change with different  $n$  and  $m$  and how does it depend on  $\sigma$ , the standard deviation of the observations drawn via bootstrap or using a parametric distribution? Answers to these questions will help a researcher implement the KROM algorithm in practice.

To provide at least indicative answers, we perform an experiment by drawing  $z_{ij}$  independently

from  $\mathcal{N}(0, \sigma^2)$ , setting the target  $\boldsymbol{\tau}_n = \mathbf{0}_n$  for consistency, because we know from Appendix C that one should use another distribution, such as the skew normal, the normal inverse Gaussian or the beta distribution, when the target Kollo skewness is not zero. Table 2 reports the results using 10,000 normal simulations, for different pairs  $(n, m)$ . Because the computational time increases with  $m$ , we simply report the proportion of these 10,000 draws for which the Kollo skewness equations have no solution. If this is 100% then the algorithm might even fail completely however many draws from  $\mathcal{N}(0, \sigma^2)$  are used. We also report the proportion of draws from a normal distribution for which Lemma 1 holds, i.e. the inequality (17) is valid. This is because, for the first column,  $j = 1$ , there is an additional cubic equation (16-3) which is the most difficult one to solve. For simplicity, Table 2 only reports results for values based on  $\mathcal{N}(0, \sigma^2)$  with the same  $\sigma$  for each column. To examine the effect of the system dimension, we set  $n = 5$  and  $n = 20$ .

**Table 2: Proportion of Draws from  $\mathcal{N}(0, \sigma^2)$  Yielding No Real Solutions to Kollo Skewness Equations.** The values for  $z_{ij}$  are independently drawn 10,000 times from  $\mathcal{N}(0, \sigma^2)$  and the table reports the proportion of draws for which the Kollo skewness equations (15-1) – (15-4) have no solution, i.e. the conditions of Theorem 1 do not hold. We also denote by  $\alpha_1$  the proportion of draws for which the inequality of Lemma 1 does not hold. We set  $n = 5$  and  $n = 20$ , and  $\boldsymbol{\tau}_n = \mathbf{0}_n$  for different  $n$  and for different simulation sample sizes  $m = 50, 100, 500, 1000$ . We let  $\sigma^2$  vary from 0.6 to 0.9.

$n$	$\boldsymbol{\tau}_n = \mathbf{0}_n$	$\sigma^2$	$m = 50$		$m = 100$		$m = 500$		$m = 1000$	
			$\alpha_1$	$\alpha$	$\alpha_1$	$\alpha$	$\alpha_1$	$\alpha$	$\alpha_1$	$\alpha$
5	$\mathbf{0}_5$	0.6	0	0.62	0	0.40	0	0.17	0	0.23
		0.7	0.31	12.34	0	1.74	0	0.18	0	0.29
		0.8	10.83	70.80	1.25	38.67	0	0.51	0	0.16
		0.9	49.83	99.50	34.65	98.69	0.10	53.51	0	14.68
20	$\mathbf{0}_{20}$	0.6	0.01	63.56	0	28.06	0	0.63	0	0.18
		0.7	0.44	99.78	0.01	99.36	0	1.74	0	0.15
		0.8	10.86	100	1.03	100	0	98.73	0	25.52
		0.9	49.49	100	34.50	100	0.06	100	0	100

For any given  $m$  and  $n$  in Table 2, the following properties are observed: all draws from any normal distribution yield real roots for the first column, that is, the inequality condition (17) of Lemma 1 always holds, especially for low values of  $\sigma^2$ ; this is not affected by the dimension  $n$  of the system but (17) becomes less likely to hold as  $\sigma^2$  increases; and finally, as either  $n$  or  $\sigma^2$  increases, the entire system of Kollo skewness equations also becomes more difficult to solve – e.g. when  $\sigma^2 = 0.9$  it is highly probable that the KROM algorithm will not work for  $n = 20$  or more. These results provide a numerical answer to the question of how small  $\sigma^2$  should be, given the dimension of the system and the number of simulations in each sub-sample, prior to concatenation.

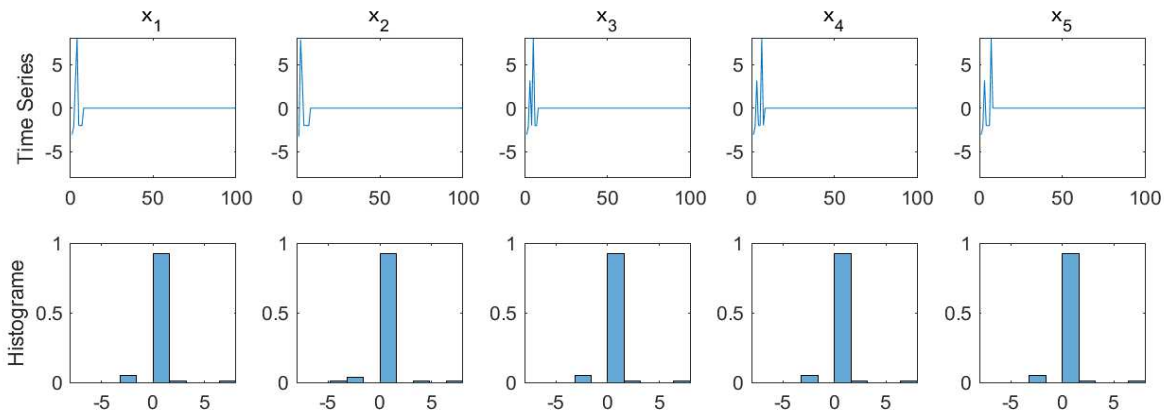
If time is not an issue, the prolonged ‘trial-and-error’ generation of arbitrary values in the Hanke et al. (2017) algorithm may be acceptable. However, in some applications it can be important to perform a very large number of simulations in an extremely short time – for instance, when pricing financial products in an algorithmic trading strategy. In that case, we may wish to define a prescribed acceptable failure rate  $\alpha$ , e.g.  $\alpha = 0.05$ . When might a prescribed failure rate be useful? Much depends whether on the time taken for the algorithm to work, which itself depends on the dimension of the system and the number of simulations in each sub-sample. For instance, using the code that we provide with this paper, running Python under Windows on a computer with Intel Core i5-8250U CPU, 3.41 GHz, and 8 GB RAM, it takes only 0.0375 seconds to generate 1000

simulations for a 20-dimensional system, but this is using zero arbitrary values when  $\tau_n = \mathbf{0}_n$ . It takes 1.956 seconds to generate the same number of simulations when drawing from  $\mathcal{N}(0, 0.5)$  and 4.706 seconds with  $\mathcal{N}(0, 0.8)$ . These times increase rapidly with  $n$  especially when the target Kollo skewness is larger.

In practice, we utilise sample concatenation to improve the statistical features of ROM simulations. For instance, consider the extreme case where all arbitrary values for  $n$  variables are zero so that a direct application of the Hanke et al. (2017) algorithm yields only  $n + 2$  rows with non-zeros values. This results in some strange features especially when the simulation size  $m$  is large. To see this, consider an hypothetical example with  $n = 5$ ,  $m = 100$ , a target mean vector  $\mathbf{0}_5$ , a target covariance matrix  $\mathbf{1}_5$  and Kollo skewness vector  $\mathbf{1}_n$ . Figure 1 plots the resulting sequential graphs and histograms for the corresponding ROM simulations.

Clearly, the Kollo skewness structure is captured by the first few elements alone – the rest of the simulation is zero. If required, application of a random permutation matrix in the ROM simulation can change the location of this activity, as discussed in Ledermann et al. (2011), but such patterns are not appropriate in many fields of application. Nevertheless, [setting arbitrary values to zero does have one advantage – it reduces the failure rate.](#)

Figure 1: **Samples Generated by the Hanke et al. (2017) Algorithm with Zero Arbitrary Values.** Setting  $m = 100$ ,  $n = 5$ ,  $\tau = \mathbf{1}_5$  and depicting sequential figures (above) and histograms (below).

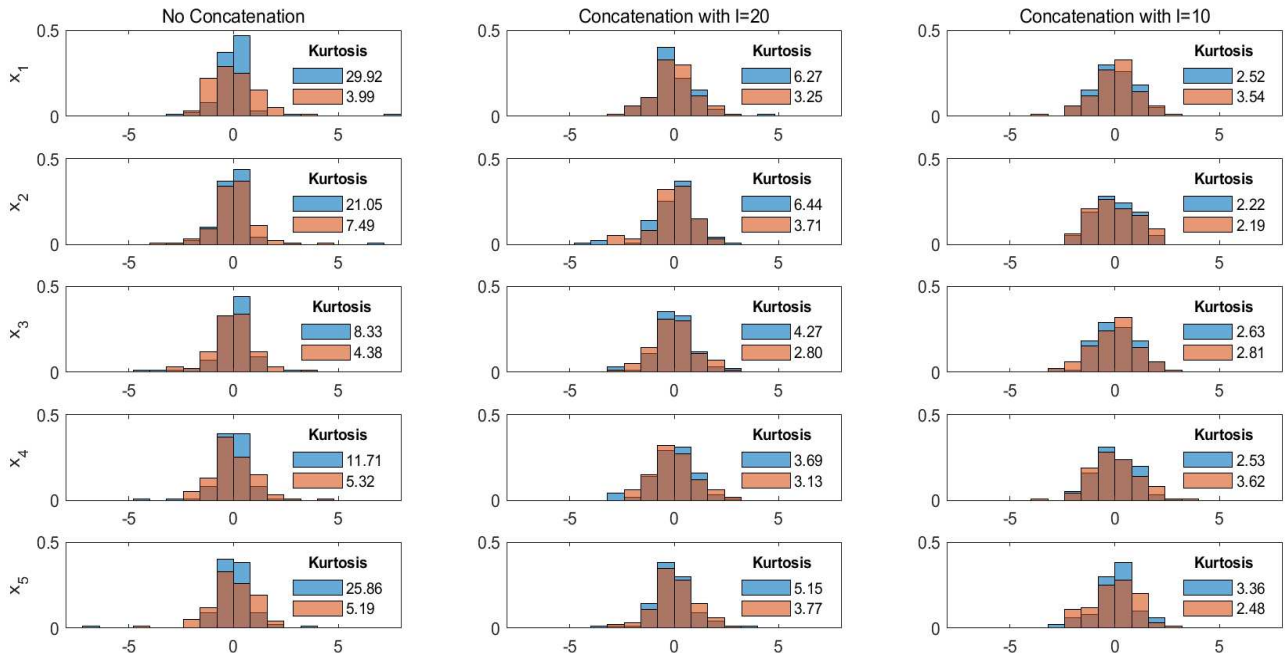


In KROM simulation applications, such as those in finance, we advocate using a bootstrap rather than a parametric distribution to populate the undetermined values of the Kollo skewness equations, for reason which shall presently become clear. However, because we always need to apply a variance reduction in equation (21) to ensure admissibility of the values selected, excessively high kurtosis could be problem for some applications, and this is where we advocate the use of the concatenation option. To illustrate just how high the kurtosis can be, and how concatenation reduces this, compare choosing arbitrary values from  $\mathcal{N}(0, 0.3)$  with those from  $\mathcal{N}(0, 0.6)$ , otherwise setting the same parameters as those for Figure 1. The first column of Figure 2 exhibits the corresponding histograms of KROM simulations. The results for  $\sigma^2 = 0.3$  in blue show many extreme values and a much greater kurtosis than the result for  $\sigma^2 = 0.6$  in orange. Next, we apply concatenation, splitting  $m$  into  $N$  blocks, and applying the KROM algorithm separately for each block. The histograms in the middle and right-hand columns of Figure 2 depict the histograms

obtained using sub-sample sizes 10 and 20. The figures also display the corresponding marginal kurtosis. Without concatenation, marginal kurtosis is extremely high especially using  $\mathcal{N}(0, 0.3)$  (blue). In each case and for each variable, concatenation reduces this, especially when the sub-sample size in the concatenation is small.

Figure 2: **The Effect of Concatenation in KROM Simulation**

The left-hand column shows the results generated by the basic KROM algorithm with  $n = 5$ ,  $m = 100$ ,  $\tau = 1_5$  and the other columns show the effect of the concatenation extension. With concatenation, the length of the sub-samples are  $l = 20$  (middle column) and  $l = 10$  (right-hand column). The rows correspond to variables  $x_1, \dots, x_5$ . The blue and orange shows the sample using two normal distributions,  $\mathcal{N}(0, 0.3)$  (blue) and  $\mathcal{N}(0, 0.6)$  (orange).



## 4 Empirical Study

Here we illustrate the application of KROM simulation to two different systems of financial returns, based on real data. Section 4.1 examines the empirical time series and cross-sectional properties of the Kollo skewness vector and its rotation. Section 4.2 demonstrates the usefulness of KROM simulation using bootstrapping compared with drawing simulations from a parametric distribution. Section 4.3 investigates the sampling errors for mean, covariance and Kollo skewness when a standard bootstrap is applied. The size and significance of these errors validates one of the main advantages of our algorithm which, of course, always has zero sampling error by design.

### 4.1 Kollo Skewness Properties of Financial Data

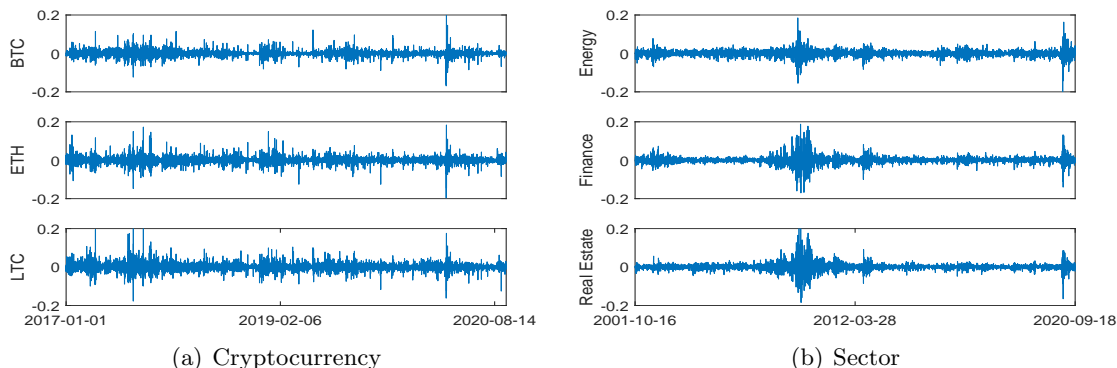
We consider two systems of returns depicted in Figure 3. On the left are hourly returns on US dollar prices of three cryptocurrencies: bitcoin (BTC), ether (ETH), and litecoin (LTC) from 1 January 2017 to 14 August 2020, over 27,000 data points in each series. The other data set is for eleven S&P 500 industry sector indices consisting of companies in the same or related industries.



Here we employ daily returns from 16 October 2001 to 18 September 2020 and there are over 4,500 data points in each series. The right panel of Figure 3 only depicts three of the eleven indices, viz. Energy, Finance and Real Estate.

**Figure 3: Time Series of Financial Returns.**

Panel (a) exhibits the hourly returns on three cryptocurrencies: BTC, ETH and LTC and panel (b) exhibits the daily returns for three S&P 500 sector indices, viz. Energy, Finance and Real Estate



First we calculate the Kollo skewness vector using a rolling window to illustrate the range of values that could be expected using real data. For the hourly cryptocurrency data, setting the length of rolling window 720 points (i.e. around one month) all elements in the Kollo skewness vector lie in the range  $[-10, 10]$  with most sampling variability in  $\tau_1$ , as shown in panel (a) of Figure 4. In particular, the cryptocurrency market-wide price crash on 12 January 2020 (Black Thursday) is evident from the dip in Kollo skewness down to almost  $-10$ . On the right, panel (b) of Figure 4 depicts the rotated Kollo skewness using the matrix  $\Omega_n$  specified in Section 3.2. Here we note that  $p_1, p_2$  and  $p_3$  almost always lie in the range  $[-3, 3]$ .

**Figure 4: Kollo Skewness and its Rotation for the Cryptocurrency Hourly Returns.**

The Kollo skewness and its rotation are computed on a rolling window of 720 hourly returns.

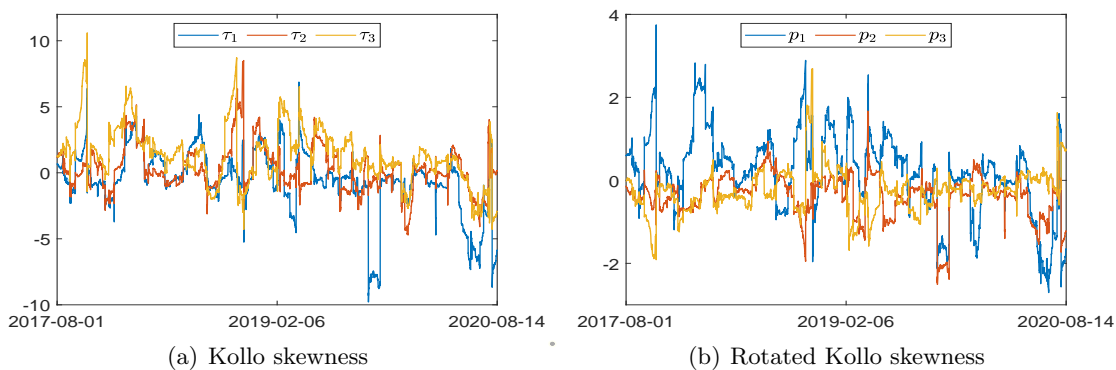
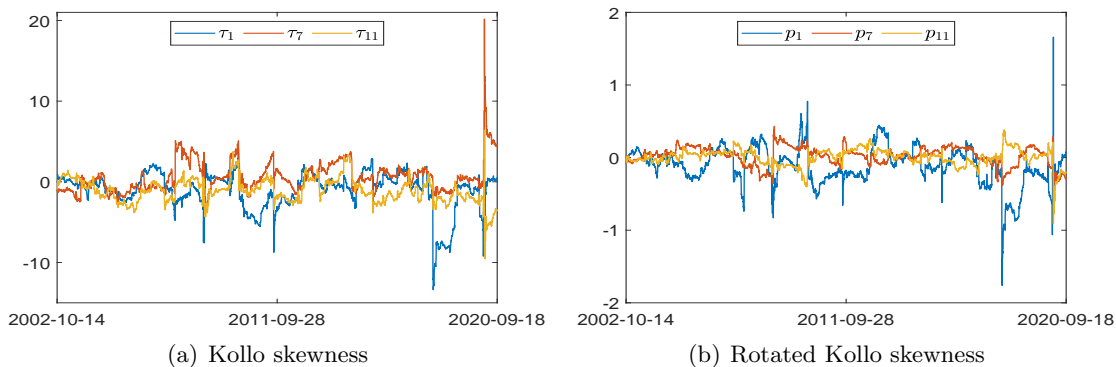


Figure 5 illustrates the results of similar computations for the S&P 500 sector data, this time using a one-year rolling window containing 250 points. To keep consistency with Figure 3 we only depict  $\tau_1, \tau_7$  and  $\tau_{11}$ , i.e. the Energy, Finance and Real Estate sector results, but the 11-dimensional

Kollo skewness and its rotated value are in a similar range for the other sectors. The Kollo skewness takes a very similar range to the cryptocurrency data except during the sector-wide crash in the S&P 500 index in March 2020. For example the low values of  $\tau_1$  during the first half of 2018 were caused by an upward surge in oil prices. Similarly, the upward spike in  $\tau_7$  on 16 March 2020 resulted from an extreme return in the Finance sector index, of around  $-14\%$ . Apart from these extreme values, we note that most elements in the rotated Kollo skewness lie in the range  $[-1, 1]$ .

**Figure 5: The Energy, Finance and Real Estate elements of Kollo Skewness and its Rotation**

Based on the daily returns of eleven S&P 500 sector indices, we depict only three. The Kollo skewness and its rotation are computed on a rolling window of 250 daily returns.



## 4.2 Applications of KROM Simulation

Next we apply the KROM algorithm to simulate the three-dimensional cryptocurrency hourly returns, based on some historical values for mean, covariance and Kollo skewness, i.e. certain empirical quantiles derived from the sample exhibited in Figure 4. We design the experiment with extreme values and a median value by selecting target samples with corresponding 1%, 50% and 99% quantiles of  $p_1$ . We focus on the first element of  $\mathbf{p}_n$  because the most strict conditions are the cubic restriction on the first column of  $\mathbf{S}_{mn}$ , i.e. equation (15-1). That is, the  $p_1$  time series exhibited in Figure 4 panel (b) is used to generate a histogram and the  $q$ -quantile is identified from this, for  $q = 1\%, 50\%$  and  $99\%$ . For each quantile of  $p_1$ , the corresponding values for  $p_2$  and  $p_3$  are those observed for the same time period, based on same 720 observations for each variable. These  $\mathbf{p}_3$  vectors are named Case 1, Case 2, and Case 3 in the left-hand column of Table 3.

To demonstrate that the KROM algorithm works best when we use a bootstrap from a real data sample to solve the Kollo skewness equations, we compare this approach to using some parametric distributions, viz. the normal distribution (N), the skew-normal (SN), the beta (Beta), and the normal inverse Gaussian distribution (NIG). In each case we set  $\sigma^2$  to either 0.7, 0.8 and 0.9 and fix the other parameters by fitting to each sample of 720 observations for each variable. This way, the distributions are parametrised to reflect the properties of each marginal empirical distribution. Table 3 reports the results, in terms of the proportion of 10,000 trials for which we cannot find a solution to the Kollo skewness equations. The table reports this for different values of  $\tau_3$ ,  $m$  and  $\sigma$  as defined in (21). The parameters of each distribution are fixed throughout.

**Table 3: KROM Simulation: Bootstrapping from Real Data vs Drawing from Parametric Distributions**

We report the proportion among 10,000 trials where the Kollo Skewness equations cannot be solved. That is, the necessary and sufficient conditions in Theorem 1 do not hold. The three target samples with different Kollo skewness are obtained using historical data and these are rotated using the matrix defined in Section 3. We apply KROM to simulate samples of size  $m = 500$  and  $m = 1000$  and compare the different ways of generating values for the Kollo skewness equations: bootstrapping from historical data, assuming a normal distribution (Normal), a skewed-Normal distribution (SN), a Beta distribution (Beta), and a Normal-Inverse Gaussian distribution (NIG), each computed for different values of  $\sigma$  in (21).

	$\tau_3$	$\tilde{\tau}_3$	$\sigma^2$	Bootstrapping		Normal		SN		Beta		NIG	
				500	1000	500	1000	500	1000	500	1000	500	1000
1	$\begin{bmatrix} -6.44 \\ -2.22 \\ -2.97 \end{bmatrix}$	$\begin{bmatrix} -2.24 \\ -1.05 \\ 0.18 \end{bmatrix}$	0.7	35.62	7.56	100	97.93	96.83	0.01	0.08	0.18	36.79	4.97
			0.8	68.23	36.80	100	100	100	100	95.43	1.52	79.41	44.90
			0.9	83.67	75.13	100	100	100	100	99.98	99.91	90.63	84.63
2	$\begin{bmatrix} -1.09 \\ 1.25 \\ 1.08 \end{bmatrix}$	$\begin{bmatrix} 0.24 \\ -0.61 \\ 0.04 \end{bmatrix}$	0.7	34.99	31.97	0.01	0.02	1.85	0.53	0.94	0.27	38.77	34.60
			0.8	35.31	31.18	0.65	0.02	2.02	0.53	1.32	0.41	39.35	35.28
			0.9	46.84	46.67	100	97.86	76.44	71.77	79.28	73.18	57.59	54.07
3	$\begin{bmatrix} 2.47 \\ 3.82 \\ 5.90 \end{bmatrix}$	$\begin{bmatrix} 2.35 \\ -0.65 \\ -0.49 \end{bmatrix}$	0.7	44.52	9.44	100	100	99.72	0.03	0.14	0.39	37.85	4.75
			0.8	57.12	33.61	100	100	100	100	51.79	1.34	67.74	38.98
			0.9	74.57	69.05	100	100	100	100	99.51	99.32	87.65	82.21

As anticipated from our numerical results in Section 3.3 the smallest failure rates occur for larger  $m$  and smaller  $\sigma^2$ . In addition, we find that extremely skewed data (Case 1 and Case 3) yields a substantially higher failure rate than moderately skewed data (Case 2). Of all methods for generating arbitrary values the historical bootstrap has the most stable performance and much the lowest failure rate except when  $m$  is large and  $\sigma^2$  is small. Comparing the failure rate for the parametric distributions, as expected we find the normal distribution only works well around the median range, i.e. when the rotated Kollo skewness is about  $\mathbf{0}$ . Clearly, Table 3 suggests that bootstrapping from a historical sample (when possible) produces the lowest failure rates in general. This is not surprising, and in fact, in some sense tautological: the simulations generated using historical data should retain most of the properties of that data.

There are many potential applications of KROM simulation to financial risk analysis. Standard parametric or bootstrap simulation methods are often used to measure quantile-based risk metrics such as value-at-risk (Duffie and Pan, 1997). However, the considerable simulation error inherent in these approaches can distort results. In an attempt to reduce this risk, a very large number of time-consuming simulations are commonly used, especially when measuring risk in large systems (Jorion, 1996). However, the focus is usually on reducing errors in the simulated covariance matrix only, ignoring errors in higher moments. In the next sub-section we demonstrate that bootstrap simulation errors in Kollo skewness are even greater than those for the covariance matrix, so both parametric and bootstrap versions of KROM simulation methods have great advantages for quantile risk measurement. KROM methods are able to simultaneously target both Kollo skewness and covariance matrices exactly, this way generating precise risk measures at each and every simulation.

Another application is to stress testing portfolios. Recall that the bootstrap version of the KROM algorithm first standardizes all returns to have zero mean and unit variance, and then applies a variance shrinkage parameter  $\sigma^2$  in (21). Because lower values of  $\sigma^2$  are more efficient, Kollo

skewness targeting is well suited to Cases 1 and 3, i.e. where the target vector corresponds to stressful periods represented by the 1% or 99% quantiles of the historical Kollo skewness distributions. Then, the other observations that are bootstrapped would correspond to more normal market conditions. This way, based on a rolling window over each (possibly concatenated) KROM simulation, one could construct a time-varying series of risk metrics. Kollo skewness is flexible because it only requires target moments so it is convenient for all forms of scenario analyses, not only stress testing.

Clearly, KROM simulation can be useful for computing minimum required capital for market risk in banks. Under the Basel II Accord, this capital depends on quantile risk metrics linked to both normal and stressed market conditions. It also has potential applications to portfolio optimization when the allocation problem aims to maximise expected profits whilst minimising some risk metric. For example, Ledermann (2010) analyses the portfolio allocation problem with a mean plus quantile-based selection criterion. Although that application uses standard ROM simulation, one could also use KROM simulation to incorporate the co-skewness between different assets in the optimization objective.

### 4.3 Sampling Errors from Standard Bootstrapping

We emphasize that using KROM simulation with bootstrapping from real data is fundamentally different from the standard bootstrap approach. When targeting the mean, covariance matrix and Kollo skewness vector, our method has zero sampling error in each and every KROM simulation. However, a standard bootstrap approach would inevitably suffer from sampling errors. To illustrate the advantage of the KROM approach we now examine these sampling errors using a root mean square error (RMSE). For any given  $n$ , if  $\mu_i, V_{ij}, \tau_i$  are the elements of the target mean  $\boldsymbol{\mu}_n$ , covariance  $\mathbf{V}_n$  and Kollo skewness  $\boldsymbol{\tau}_n$  respectively and  $\hat{\mu}_i, \hat{V}_{ij}, \hat{\tau}_i$  are the corresponding elements of the sample moments obtained by standard bootstrapping, the RMSE are defined, respectively, by:

$$\sqrt{\sum_i^n (\mu_i - \hat{\mu}_i)^2}, \sqrt{\sum_{i,j} (V_{ij} - \hat{V}_{ij})^2}, \sqrt{\sum_i^n (\tau_i - \hat{\tau}_i)^2}. \quad (23)$$

Table 4 reports sampling errors for the mean vector, covariance matrix and Kollo skewness vector when applying the statistical bootstrapping to the cryptocurrency historical returns. Again we set rotated Kollo skewness to Cases 1, 2 and 3 as described above for Table 3. Note that 720 hourly returns were used to generate each  $q$ -quantile. It is these returns that we use for each case of the statistical bootstrap. This way, we know the multivariate sample moments and we use 720 data points to bootstrap samples of a fixed size  $m$ , with replacement. We consider sample sizes  $m = 100, 500$  and  $1000$ . In order to preserve correlation, we randomly select entire rows of the target sample. We do 10,000 bootstraps so the RMSE above are calculated 10,000 times, and this way we obtain both a mean and a standard error of each quantity in (23). The right-hand panel of Table 4 reports the ratio of the mean to the standard error, using the central limit theorem to derive critical values for significance. The results show that sampling errors are very significant for both the mean and Kollo skewness, especially when  $m$  is small.

Table 4: **RMSE of Multivariate Moments in Standard Statistical Bootstrapping.**

The first three columns illustrate the first three moments for three sets of samples each of size 720 and the fourth column states the size of each bootstrap. The mean and standard error (in parentheses, below) derived using (23) are in columns 5–7, computed using 10,000 bootstraps for each. The last three columns are the ratio of the average RMSE to its standard error and we use \*, \*\* or \*\*\* to denote significantly greater than 0 at the 90%, 95% or 99% confidence level, respectively.

$\mu_3$ ( $10^{-5}$ )	$\mathbf{V}_3$ ( $10^{-5}$ )	$\tau_3$	$m$	$\mu_3(10^{-5})$	RMSE $\mathbf{V}_3(10^{-5})$	$\tau_3$	$\mu_3$	Ratio $\mathbf{V}_3$	$\tau_3$
$\begin{bmatrix} 6.91 \\ 20.53 \\ 0.06 \end{bmatrix}$	$\begin{bmatrix} 2.93 & 2.99 & 2.74 \\ 2.99 & 4.40 & 3.49 \\ 2.74 & 3.49 & 3.65 \end{bmatrix}$	$\begin{bmatrix} -6.44 \\ -2.22 \\ -2.97 \end{bmatrix}$	100	8.739 (5.827)	5.017 (3.855)	7.409 (3.131)	1.500*	1.302*	2.367***
			500	3.939 (2.449)	2.303 (1.624)	4.563 (2.875)	1.608*	1.418*	1.587*
			1000	2.823 (1.746)	1.607 (1.126)	3.141 (2.072)	1.617*	1.427*	1.516*
$\begin{bmatrix} -4.11 \\ 14.12 \\ -2.31 \end{bmatrix}$	$\begin{bmatrix} 2.61 & 2.59 & 2.52 \\ 2.59 & 4.74 & 3.96 \\ 2.52 & 3.96 & 5.51 \end{bmatrix}$	$\begin{bmatrix} -1.09 \\ 1.25 \\ 1.08 \end{bmatrix}$	100	9.834 (5.817)	3.927 (2.989)	3.731 (1.735)	1.691**	1.314*	2.150**
			500	4.379 (2.506)	1.830 (1.193)	2.652 (1.188)	1.747**	1.534*	2.232**
			1000	3.111 (1.786)	1.301 (0.859)	1.892 (1.028)	1.742**	1.514*	1.841**
$\begin{bmatrix} -21.09 \\ 86.00 \\ -21.58 \end{bmatrix}$	$\begin{bmatrix} 26.56 & 25.41 & 27.88 \\ 25.41 & 43.41 & 32.83 \\ 27.88 & 32.83 & 41.75 \end{bmatrix}$	$\begin{bmatrix} 2.47 \\ 3.82 \\ 5.90 \end{bmatrix}$	100	28.530 (17.091)	28.750 (23.705)	7.314 (3.003)	1.669**	1.213	2.435***
			500	12.836 (7.634)	13.782 (9.385)	4.790 (2.365)	1.681**	1.469*	2.026**
			1000	9.114 (5.445)	9.768 (6.710)	3.270 (2.104)	1.674**	1.456*	1.554*

## 5 Summary and Conclusions

The existing ROM simulation algorithm that can produce multivariate sample having exact Kollo skewness proceeds by solving a system of simultaneous non-linear equations numerically, in an iterative manner. Because the system is under-determined, the simulations are generated from a very large number of so-called ‘arbitrary’ values. However, the trial-and-error approach to finding arbitrary values that the authors advocate may fail, and even when it works the algorithm is relatively slow. Furthermore, it produces simulations with very long periods of inactivity and excessively high kurtosis, and so it is difficult to find any real-world application except, perhaps, to specific problems in seismic wave dynamics or cardiology.

This paper introduces a new methodology for ROM simulation to target Kollo skewness, which we call KROM simulation [which proceeds in three stages](#). The first replaces the slow, trial-and-error approach with a rapid check of new, necessary and sufficient conditions for the Kollo skewness equations to have real solutions. The second stage utilizes a bootstrap, if possible and otherwise draws simulations from a parametric distribution, in order that that the simulations exhibit realistic sample characteristics. An optional third stage applies sample concatenation to reduce marginal kurtosis, if desired. The algorithm utilizes and is supported by several new theoretical results, which are proved in the appendices. We also present some detailed numerical analysis on failure rates as well as an empirical study that applies the KROM algorithm to real financial data. By examining how the failure rate depends on the dimension of the system, the number of simulations, the number of sub-samples, and the characteristics of the empirical or parametric distributions, we

are able to guide the researcher how best to operate KROM simulation by setting sample sizes, and by selecting distributions and choosing their parameter values. To the best of our knowledge our empirical study is the first application of Kollo skewness to financial data. After describing the sample characteristics of Kollo skewness it focuses on the features of KROM simulation that appeal to risk management and portfolio optimization applications. We outline the design of such a methodology but its actual implementation in practice is a subject for later research.

## References

- Adelfio, G., Chiodi, M., D'Alessandro, A., Luzio, D., D'Anna, G., and Mangano, G. (2012). Simultaneous seismic wave clustering and registration. *Computers & Geosciences*, 44:60–69.
- Alexander, C. and Ledermann, D. (2012). ROM simulation: Applications to stress testing and VaR. *Available at SSRN 2049239*.
- Avramidis, A. and Matzinger, H. (2002). Convergence of the stochastic mesh estimator for pricing American options. *Winter Simulation Conference Proceedings*, 2:1560–1567.
- Badano, A. and Samuelson, F. (2013). Uncertainty of Monte Carlo variance estimates: Application to the simulation of x-ray imaging detectors. *Progress in Biomedical Optics and Imaging - Proceedings of SPIE*, 8668.
- Balakrishnan, N., Brito, M., and Quiroz, A. (2007). A vectorial notion of skewness and its use in testing for multivariate symmetry. *Communications in Statistics-Theory and Methods*, 36(9):1757–1767.
- Bollerslev, T., Engle, R. F., and Nelson, D. B. (1994). Arch models. *Handbook of econometrics*, 4:2959–3038.
- Capriotti, L. (2008). Least-squares importance sampling for Monte Carlo security pricing. *Quantitative Finance*, 8(5):485–497.
- Cardano, G. (1968). *Ars Magna or the Rules of Algebra*. Dover Publications.
- Duffie, D. and Pan, J. (1997). An overview of value at risk. *Journal of Derivatives*, 4(3):7–49.
- Engle, R. F. (1982). Autoregressive conditional heteroscedasticity with estimates of the variance of United Kingdom inflation. *Econometrica: Journal of the Econometric Society*, pages 987–1007.
- Ferraz, V. and Moura, F. (2012). Small area estimation using skew normal models. *Computational Statistics and Data Analysis*, 56(10):2864–2874.
- Geyer, A., Hanke, M., and Weissensteiner, A. (2014). No-arbitrage ROM simulation. *Journal of Economic Dynamics and Control*, 45:66–79.
- Golub, G. H. and Van Loan, C. F. (2012). *Matrix Computations*, volume 3. JHU press.
- Gutjahr, S., Henze, N., and Folkers, M. (1999). Shortcomings of generalized affine invariant skewness measures. *Journal of Multivariate Analysis*, 71(1):1–23.
- Hanke, M., Penev, S., Schief, W., and Weissensteiner, A. (2017). Random orthogonal matrix simulation with exact means, covariances, and multivariate skewness. *European Journal of Operational Research*, 232(2):510–523.
- Hesterberg, T. (1996). Control variates and importance sampling for efficient bootstrap simulations. *Statistics and Computing*, 6(2):147–157.
- Hürlimann, W. (2013). Generalized Helmert–Ledermann orthogonal matrices and ROM simulation. *Linear Algebra and its Applications*, 439(7):1716–1729.

- Hürlimann, W. (2014). Market Value-at-Risk: ROM simulation, Cornish-Fisher VaR and Chebyshev-Markov VaR bound. *British Journal of Mathematics & Computer Science*, 4(13):1797.
- Hürlimann, W. (2015). On Mardia skewness and kurtosis of Soules basis matrices in ROM simulation. *Linear Algebra and its Applications*, 473:284–296.
- Jammalamadaka, S. R., Taufer, E., and Terdik, G. H. (2020). On multivariate skewness and kurtosis. *Sankhya A*, pages 1–38.
- Joanes, D. and Gill, C. (1998). Comparing measures of sample skewness and kurtosis. *Journal of the Royal Statistical Society: Series D (The Statistician)*, 47(1):183–189.
- Jorion, P. (1996). Risk2: Measuring the risk in value at risk. *Financial Analysts Journal*, 52(6):47–56.
- Kollo, T. (2008). Multivariate skewness and kurtosis measures with an application in ICA. *Journal of Multivariate Analysis*, 99(10):2328–2338.
- Ledermann, D. (2010). *Random orthogonal matrix simulation with financial applications*. PhD thesis, The University of Reading.
- Ledermann, D. and Alexander, C. (2012). Further properties of random orthogonal matrix simulation. *Mathematics and Computers in Simulation*, 83:56–79.
- Ledermann, W., Alexander, C., and Ledermann, D. (2011). Random orthogonal matrix simulation. *Linear Algebra and its Applications*, 434(6):1444–1467.
- Lyon, A., Mincholé, A., Martínez, J. P., Laguna, P., and Rodriguez, B. (2018). Computational techniques for ecg analysis and interpretation in light of their contribution to medical advances. *Journal of The Royal Society Interface*, 15(138):20170821.
- Ma, J. and He, P. (2016). Fast Monte Carlo simulation for pricing covariance swap under correlated stochastic volatility models. *IAENG International Journal of Applied Mathematics*, 46(3):336–345.
- Mardia, K. V. (1970). Measures of multivariate skewness and kurtosis with applications. *Biometrika*, 57(3):519–530.
- McSharry, P. E., Clifford, G. D., Tarassenko, L., and Smith, L. A. (2003). A dynamical model for generating synthetic electrocardiogram signals. *IEEE Transactions on Biomedical Engineering*, 50(3):289–294.
- Móri, T. F., Rohatgi, V. K., and Székely, G. (1994). On multivariate skewness and kurtosis. *Theory of Probability & Its Applications*, 38(3):547–551.
- Oberkampf, W. L., DeLand, S. M., Rutherford, B. M., Diegert, K. V., and Alvin, K. F. (2002). Error and uncertainty in modeling and simulation. *Reliability Engineering & System Safety*, 75(3):333–357.
- Quintana, C., Millwater, H., Singh, G., and Golden, P. (2015). Optimal allocation of testing resources for statistical simulations. *Engineering Optimization*, 47(7):979–993.
- Saliby, E. and Paul, R. (2009). A farewell to the use of antithetic variates in Monte Carlo simulation. *Journal of the Operational Research Society*, 60(7):1026–1035.
- Swain, J. and Schmeiser, B. (1988). Control variates for Monte Carlo analysis of nonlinear statistical models, II: raw moments and variances. *Journal of Statistical Computation and Simulation*, 30(1):39–56.
- Szántai, T. (2000). Improved bounds and simulation procedures on the value of the multivariate normal probability distribution function. *Annals of Operations Research*, 100:85–101.

Takanami, T. and Kitagawa, G. (1991). Estimation of the arrival times of seismic waves by multi-variate time series model. *Annals of the Institute of Statistical Mathematics*, 43(3):407–433.

Thomopoulos, N. T. (2012). *Essentials of Monte Carlo Simulation: Statistical Methods for Building Simulation Models*. Springer Science & Business Media.

## Appendix

### A Proofs

*Proof of Lemma 1.* For convenience, let us re-write the system (16-1)–(16-3) as follows:

$$\begin{aligned} s_{11} + s_{21} + s_{31} &= - \sum_{i=4}^m w_{i1} =: a, \\ s_{11}^2 + s_{21}^2 + s_{31}^2 &= m - \sum_{i=4}^m w_{i1}^2 =: b, \\ s_{11}^3 + s_{21}^3 + s_{31}^3 &= mp_1 - \sum_{i=4}^m w_{i1}^3 =: c. \end{aligned}$$

Let  $x_1 = s_{11} - \frac{a}{3}$ ,  $x_2 = s_{21} - \frac{a}{3}$  and  $x_3 = s_{31} - \frac{a}{3}$ . Then, the above equations reduce to:

$$x_1 + x_2 + x_3 = 0, \tag{A.1}$$

$$x_1^2 + x_2^2 + x_3^2 = b - \frac{a^2}{3} =: d, \tag{A.2}$$

$$x_1^3 + x_2^3 + x_3^3 = c - ab + \frac{9}{2}a^3 =: e. \tag{A.3}$$

We want to establish the conditions under which the system of equations has real roots. After eliminating  $x_2$  and  $x_3$ , we obtain

$$6x_1^3 - 3dx_1 - 2e = 0. \tag{A.4}$$

This is a cubic equation for  $x_1$  and always has a real root of the form  $x_1^* = \sqrt[3]{\frac{e}{6} + \sqrt{\Delta_3}} + \sqrt[3]{\frac{e}{6} - \sqrt{\Delta_3}}$ , where  $\Delta_3 = (e/6)^2 - (d/6)^3$  (Cardano, 1968). Substitute  $x_1^*$  in equation (A.1) and equation (A.2). Then we get a quadratic equation for  $x_2$ ,

$$x_2^2 + x_1^*x_2 + x_1^{*2} - \frac{d}{2} = 0. \tag{A.5}$$

By the simple linear equation (A.1), it is sufficient to analyse when the quadratic equation (A.5) has a real root. Using a standard result for quadratic equations, equation (A.5) has a real root if and only if the following discriminant is non-negative,

$$\Delta_2 = x_1^{*2} - 4 \times \left(x_1^{*2} - \frac{1}{2}d\right) = 2d - 3x_1^{*2}$$



After some tedious algebra, the discriminant  $\Delta_2$  can be simplified as follows:

$$\Delta_2 = 2d - 3x_1^{*2} = -3 \left( x_1^{*2} - \frac{2}{3}d \right) = -3 \left( \sqrt[3]{\frac{e}{6} + \sqrt{\Delta_3}} - \sqrt[3]{\frac{e}{6} - \sqrt{\Delta_3}} \right)^2.$$

Now we can see that  $\Delta_2 \geq 0$  if and only if  $\Delta_3 \leq 0$ :

- (i) When  $\Delta_3 = 0$ ,  $\Delta_2 = -3 \left( \sqrt[3]{\frac{e}{6}} - \sqrt[3]{\frac{e}{6}} \right)^2 = 0$ ;
- (ii) When  $\Delta_3 > 0$ ,  $\Delta_2 = -3 \left( \sqrt[3]{\frac{e}{6} + \sqrt{\Delta_3}} - \sqrt[3]{\frac{e}{6} - \sqrt{\Delta_3}} \right)^2 < 0$ ;
- (iii) When  $\Delta_3 < 0$ , there are three distinct real roots for (A.4), which may be expressed in terms of polar coordinates  $\cos \alpha \pm i \sin \alpha$ , where  $\alpha = \arccos \frac{e}{6R}$  and  $R^2 = \left(\frac{e}{6}\right)^2 - \Delta_3 = \left(\frac{d}{6}\right)^3$ . So, after some algebra,  $\Delta_2$  may be written:

$$\Delta_2 = -3 \left( \sqrt[3]{\frac{e}{6} + i\sqrt{-\Delta_3}} - \sqrt[3]{\frac{e}{6} - i\sqrt{-\Delta_3}} \right)^2 = 2d \sin^2 \frac{a}{3} > 0.$$

Recall that  $\Delta_3 = (e/6)^2 - (d/6)^3$ , hence, the necessary and sufficient condition for equation (A.5) to have a real root is  $\Delta_3 \leq 0$ , viz.  $d^3 \geq 6e^2$ . The proof is complete.  $\square$

*Proof of Theorem 1 (ii) and (iii).* Here we establish the necessary and sufficient conditions for the system (15-1)-(15-4) to be solvable when  $k = 1, \dots, n$ . The system can be expressed in matrix form, as in equations (18) and (19), i.e.  $\mathbf{U}\mathbf{y} = \mathbf{v}$  and  $\mathbf{y}'\mathbf{y} = m - \sum_{i=k+3}^m w_{ik}^2$ . First, it is easy to see that condition (ii) is a necessary and sufficient condition for the linear equation (18) to be solvable, i.e.  $\text{Rank}(\mathbf{U}) = \text{Rank}([\mathbf{U}, \mathbf{v}])$  where  $[\mathbf{U}, \mathbf{v}]$  is the augmented matrix. Next we need to focus on the quadratic equation (19). The idea is to use the linear equation (18) to identify a set of linearly independent columns  $\mathbf{U}_1$  of  $\mathbf{U}$  with full column rank, which enables us to express the rest columns  $\mathbf{U}_2$  as a linear combination of  $\mathbf{U}_1$ , then the quadratic equation (19) becomes an equation on  $\mathbf{U}_1$ . More specifically, re-write equation (18) using  $\mathbf{U}_1$  and  $\mathbf{U}_2$  as  $\mathbf{U}_1\mathbf{y}_1 + \mathbf{U}_2\mathbf{y}_2 = \mathbf{v}$ , where the vectors  $\mathbf{y}_1$  and  $\mathbf{y}_2$  contain the elements in  $\mathbf{y}$  that correspond to  $\mathbf{U}_1$  and  $\mathbf{U}_2$  respectively. Therefore, we could eliminate  $\mathbf{y}_1$  in equation (19) by  $\mathbf{y}_1 = \mathbf{U}_1^+ (\mathbf{v} - \mathbf{U}_2\mathbf{y}_2)$ , where  $\mathbf{U}_1^+ = \left(\mathbf{U}_1'\mathbf{U}_1\right)^{-1} \mathbf{U}_1'$  is a Moore-Penrose inverse of  $\mathbf{U}_1$  (Golub and Van Loan, 2012). The Moore-Penrose inverse is in fact unique in this case, as  $\mathbf{U}_1$  has the full column rank  $\mathbf{U}_1$  of  $\mathbf{U}$ . Then the quadratic equation (19) becomes

$$\mathbf{y}_2'\mathbf{G}\mathbf{y}_2 - 2\mathbf{y}_2'\mathbf{g} + \mathbf{v}' \left(\mathbf{U}_1\mathbf{U}_1'\right)^+ \mathbf{v} + \sum_{j=i+3}^m w_{ji}^2 - m = 0. \quad (\text{A.6})$$

where  $\mathbf{G} = \mathbf{I} + \mathbf{U}_2' \left(\mathbf{U}_1\mathbf{U}_1'\right)^+ \mathbf{U}_2$  and  $\mathbf{g} = \mathbf{U}_2' \left(\mathbf{U}_1\mathbf{U}_1'\right)^+ \mathbf{v}$ . After completing the square, equation (A.6) becomes:

$$\mathbf{z}'\mathbf{G}\mathbf{z} = \mathbf{g}'\mathbf{G}^{-1}\mathbf{g} - \mathbf{v}' \left(\mathbf{U}_1\mathbf{U}_1'\right)^+ \mathbf{v} - \sum_{j=i+3}^m w_{ji}^2 + m,$$

where  $\mathbf{z} = \mathbf{y}_2 - \mathbf{G}^{-1}\mathbf{g}$ . Notice that  $\mathbf{G}$  is a positive-definite matrix, hence to ensure real roots of the above equation the right side of the equation must be non-negative. Therefore we obtain the

condition (iii), viz.

$$\mathbf{g}' \mathbf{G}^{-1} \mathbf{g} - \mathbf{v}' \left( \mathbf{U}_1 \mathbf{U}_1' \right)^+ \mathbf{v} \geq \sum_{j=i+3}^m w_{ji}^2 - m.$$

□

*Proof of Corollary 1.* We show that the zero arbitrary values are admissible under very mild conditions. In fact, they are not admissible only in the highly unusual cases where the number of simulations is very small and there exists one element of the Kollo skewness vector with large magnitude. To proceed, we check whether the system (15-1)–(15-4) satisfy the conditions in use Theorem 1, column by column, when all arbitrary values are zero. When  $k = 1$  we just need to check whether zero arbitrary values satisfy condition Theorem 1 (i). In this case, we have

$$a = - \sum_{i=4}^m w_{i1} = 0, \quad b = m - \sum_{i=4}^m w_{i1}^2 = m, \quad \text{and } c = mp_1 - \sum_{i=4}^m w_{i1}^3 = mp_1.$$

Then the equation (17) becomes:

$$\left( b - \frac{a^2}{3} \right)^3 \geq 6(c - ab + \frac{9}{2}a^3)^2 \Leftrightarrow b^3 \geq 6c^2 \Leftrightarrow m^3 \geq 6m^2p_1^2 \Leftrightarrow p_1^2 \leq \frac{m}{6}. \quad (\text{A.7})$$

In practical applications,  $\frac{m}{6}$  is much larger than  $p_1^2$ , so equation (A.7) holds. For  $k = 2, \dots, n$  we need to check whether conditions Theorem 1 (ii)–(iii) are satisfied. Recall that in this case  $\mathbf{U}$  and  $\mathbf{v}$  become

$$\mathbf{U} = \begin{bmatrix} s_{11}^2 & s_{21}^2 & s_{31}^2 & 0 & 0 & \dots & 0 & 0 \\ s_{11} & s_{21} & s_{31} & 0 & 0 & \dots & 0 & 0 \\ s_{12} & s_{22} & s_{32} & s_{42} & 0 & \dots & 0 & 0 \\ \vdots & \vdots & \vdots & \vdots & \vdots & \vdots & \vdots & \vdots \\ s_{1,k-1} & s_{2,k-1} & s_{3,k-1} & s_{4,k-1} & s_{5,k-1} & \dots & s_{k+1,k-1} & 0 \\ 1 & 1 & 1 & 1 & 1 & \dots & 1 & 1 \end{bmatrix}, \quad \mathbf{v} = \begin{bmatrix} mp_k \\ 0 \\ 0 \\ \dots \\ 0 \\ 0 \end{bmatrix}.$$

Let  $\mathbf{U}_1$  be the the matrix consisting of the first  $k + 1$  columns of  $\mathbf{U}$ , then we can compute the determinant of  $\mathbf{U}_1 \mathbf{U}_1'$  as:

$$\det(\mathbf{U}_1 \mathbf{U}_1') = t(k + 1)m^{k-1},$$

where  $t = s_{11}^4 + s_{21}^4 + s_{31}^4 - m \left( \frac{m}{k+1} + p_1^2 + \dots + p_{k-1}^2 \right)$ . As  $t > 0$  by assumption, we get that  $\mathbf{U}_1$  is invertible, hence is of full row rank, which implies that  $\mathbf{v}$  must be in the span of  $\mathbf{U}_1$ . Hence Theorem 1 (ii) holds.

If the system has real solutions, the condition (iii) requires  $\mathbf{g}' \mathbf{G}^{-1} \mathbf{g} - \mathbf{v}' \left( \mathbf{U}_1 \mathbf{U}_1' \right)^+ \mathbf{v} \geq -m$ . After some algebraic computation, we get

$$\mathbf{v}' \left( \mathbf{U}_1 \mathbf{U}_1' \right)^+ \mathbf{v} = \frac{m^2 p_k^2}{t}, \quad \mathbf{G} = 1 + \frac{1}{k+1} + \frac{1}{t} \left( \frac{m}{k+1} \right)^2, \quad \mathbf{g} = -\frac{m^2 p_k}{t(k+1)},$$

and condition (iii) becomes  $\frac{t}{m} + \frac{m}{(k+1)(k+1)} \geq p_k^2$ . In practical applications,  $m$  is much larger than  $n$  and  $k \leq n$ , so this inequality always holds. Thus the proof is complete. To summarise, setting all arbitrary values to zero is admissible under very mild conditions.  $\square$

## B Further Results on Normal Arbitrary Values

Here we discuss the theoretical failure rate for the first column of  $\mathbf{S}_{mn}$ , that is  $\mathbf{s}_1 = [s_{11}, \dots, s_{m1}]'$ , when using normal arbitrary values  $s_{i1} = w_{i1}$  for  $i = 4, \dots, m$  which are drawn from  $\mathcal{N}(0, \sigma^2)$  with the mean and variance adjustment given by equation (21). This way, the arbitrary variables should follow i.i.d.  $\mathcal{N}(0, \sigma^2)$ , and we can denote these  $m - 3$  random variables  $[W_{41}, W_{51}, \dots, W_{m1}]'$ . We can calculate auxiliary variables corresponding to their first three moments:

$$\begin{aligned} M_1 &= \frac{1}{m-3} \sum_{i=4}^n (W_{i1}) = \frac{1}{m-3} \sum_{i=4}^n \left( \frac{\sigma}{s_z} (Z_j - \bar{Z}) \right) = 0 \\ M_2 &= \frac{1}{m-3} \sum_{i=4}^n (W_{i1} - M_1)^2 = \frac{1}{m-3} \sum_{i=4}^n \left( \frac{\sigma}{s_z} (Z_j - \bar{Z}) \right)^2 = \sigma^2 \\ M_3 &= \frac{1}{m-3} \sum_{i=4}^n (W_{i1} - M_1)^3 = \frac{1}{m-3} \sum_{i=4}^n \left( \frac{\sigma}{s_z} (Z_j - \bar{Z}) \right)^3 = \frac{\sum_{i=4}^n (Z_j - \bar{Z})^3}{(m-3)s_z^3} \sigma^3 \end{aligned}$$

Note that  $M_1$  and  $M_2$  are both constants, taking the values 0 and  $\sigma^2$  respectively.

By the central limit theorem (Joanes and Gill, 1998) when the simulation sample size  $m$  is large  $M_3$  has an approximate normal distribution with mean 0 and variance  $\frac{6(m-5)}{m(m-2)}\sigma^6$ . Therefore, for any arbitrary values selected this way, we have:

$$\sum_{i=4}^m w_{i1} = 0, \quad \sum_{i=4}^m w_{i1}^2 = (m-3)\sigma^2, \quad \sum_{i=4}^m w_{i1}^3 = (m-3)M_3.$$

Next we check Lemma 1 for  $[W_{41}, W_{51}, \dots, W_{m1}]'$  to see whether they are admissible. Since  $a = 0$ ,  $b = m - (m-3)\sigma^2$  and  $c = mp_1 - (m-3)M_3$  in equation (17) we can rewrite the condition as:

$$p_1q - \sqrt{\frac{m-3}{6}(q - \sigma^2)^3} \leq M_3 \leq p_1q + \sqrt{\frac{m-3}{6}(q - \sigma^2)^3} \quad (\text{B.1})$$

where  $q = \frac{m}{m-3}$ . So the probability of  $[W_{41}, W_{51}, \dots, W_{m1}]'$  being admissible is the probability of  $M_3$  lying within the range given by (B.1).

Let  $h(\sigma)$  denote the failure rate for the arbitrary values, i.e. the probability that the arbitrary values do not satisfy the condition (B.1). When  $\sigma = 0$ ,  $[W_{41}, W_{51}, \dots, W_{m1}]'$  are essentially zero. By Corollary 1 zero arbitrary values are always admissible when  $p_1^2 \leq \frac{m}{6}$ , hence we have  $h(0) = 0$ . When  $\sigma \neq 0$ , because  $M_3$  is approximately normal distributed with mean 0 and variance  $\frac{6(m-5)}{m(m-2)}\sigma^6$ , let  $\Phi(\cdot)$  and  $\varphi(\cdot)$  denote the cumulative distribution function and probability density function for a standard normal distribution, then we have

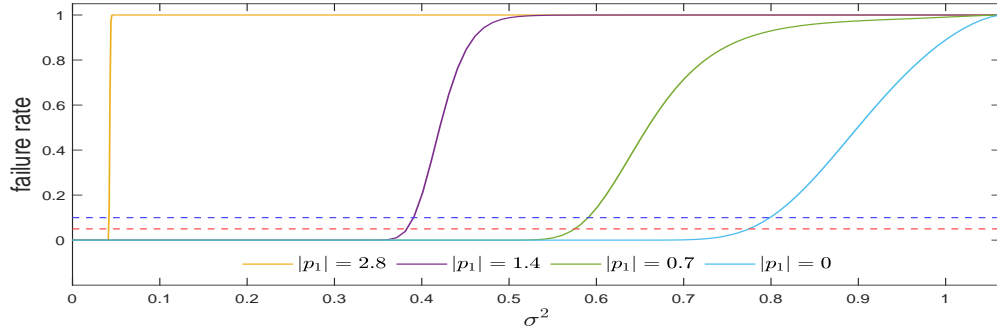
$$h(\sigma) = 1 - (\Phi(I_U) - \Phi(I_L)) \quad \text{for } 0 < \sigma \leq \sqrt{q} \quad (\text{B.2})$$

where  $I_U = \frac{1}{\sigma^3} \sqrt{\frac{m(m-2)}{6(m-5)}} \left( p_1 q + \sqrt{\frac{m-3}{6}} (q - \sigma^2)^3 \right)$  and  $I_L = \frac{1}{\sigma^3} \sqrt{\frac{m(m-2)}{6(m-5)}} \left( p_1 q - \sqrt{\frac{m-3}{6}} (q - \sigma^2)^3 \right)$ .

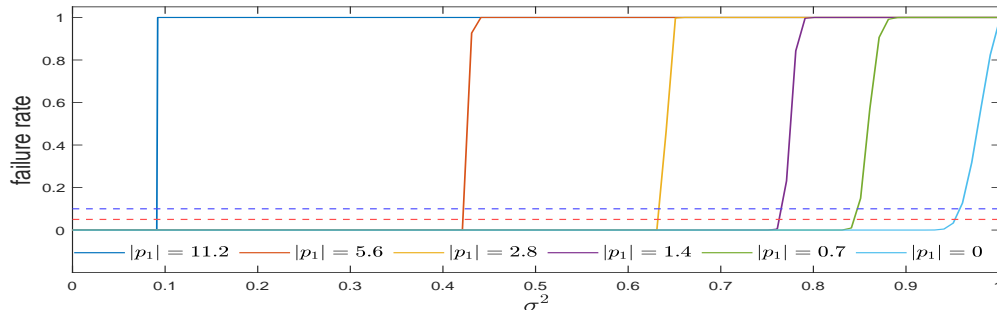
To illustrate this result, Figure 6 depicts theoretical failure rates when  $\sigma^2 \in \left[0, \frac{m}{m-3}\right]$ . for  $m = 50$  (above) and  $m = 1000$  (below) and for various value of rotated Kollo skewness between 0 and 11.2, as shown in the legend. All curves are monotonic increasing from 0 to 1 on the interval  $\sigma^2 \in \left[0, \frac{m}{m-3}\right]$  and there is an obvious jump in each curve when either  $m$  or  $|p_1|$  are large. Comparing the cases  $m = 50$  and  $m = 1000$ , for any given given failure rate  $\alpha$ , a larger sample size can allow for larger  $|p_1|$  with the same  $\sigma^2$ , or alternatively a greater  $\sigma^2$  for the same  $|p_1|$ . Therefore, when the target Kollo skewness is far away from  $\mathbf{0}_n$  we need to consider larger sizes of simulations and smaller  $\sigma^2$  to ensure a reasonably low failure rate.

Figure 6: **The Theoretical Failure Rate of the First Column with Different  $p_1$ .**

The upper plots (a) are for  $m = 50$  and those below (b) are for  $m = 1000$ . The arbitrary values in the first column are chosen from  $\mathcal{N}(0, \sigma^2)$ . The red and blue horizontal dashed line depict the failure rate at 5% and 10%.



(a)  $m = 50$



(b)  $m = 1000$

## C Attainable Skewness

This section derives new formulae for the range of skewness that can be attained using some well-known univariate distributions, and then computes this range when the distribution is standardized to have zero mean and unit variance. We provide three examples:

**Example 1** (SN distribution). The SN distribution is three-parameter distribution with PDF

$$f(t) = \frac{2}{\Omega_n} \phi \left( \frac{t - \xi}{\Omega_n} \right) \Phi \left( \alpha \left( \frac{t - \xi}{\Omega_n} \right) \right),$$

where where  $\xi$ ,  $\omega > 0$ ,  $\alpha$  are parameters;  $\phi$  and  $\Phi$  denote the PDF and CDF for the standard

Gaussian distribution with zero mean and unit variance. We can obtain the constraints OF zero mean, unit variance and  $p_1$  skewness,

$$\begin{cases} \xi + \omega\delta\sqrt{\frac{2}{\pi}} = 0 & \text{(mean)} \\ \omega^2 \left(1 - \frac{2\delta^2}{\pi}\right) = 1 & \text{(variance)} \\ \frac{\sqrt{2}(4 - \pi)\delta^3}{(\pi - 2\delta^2)^{3/2}} = p_1 & \text{(skewness)} \end{cases} \quad (\text{B.3})$$

where  $\delta = \frac{\alpha}{\sqrt{1 + \alpha^2}}$ . The skewness  $\frac{\sqrt{2}(4 - \pi)\delta^3}{(\pi - 2\delta^2)^{3/2}}$  of the SN distribution is a function of  $\alpha$ , by taking its derivative with respect to  $\alpha$ , it is not difficult to show that it is monotone increasing with respect to  $\alpha$ . Hence by passing  $\alpha$  to  $\pm\infty$ , we can show that the range of the skewness is  $(-0.995, 0.995)$ . This implies that  $\forall p_1 \in (-0.995, 0.995)$ , there always exists  $\alpha$  such that the skewness of  $Z_1$  matches  $p_1$ . Once  $\alpha$  is obtained according to skewness  $p_1$ , we can easily get  $\omega = \frac{1}{1 - \frac{2\delta^2}{\pi}}$  and  $\xi = -\omega\delta\sqrt{\frac{2}{\pi}}$  by considering the constraints for mean and variance in equation (B.3). Therefore, the attainable values of  $p_1$  are indeed  $(-0.995, 0.995)$ .

**Example 2** (NIG distribution). The NIG distribution is a four-parameter distribution, with PDF

$$f(t) = \frac{\alpha\delta K_1\left(\alpha\sqrt{\delta^2 + (t - \mu)^2}\right)}{\pi\sqrt{\delta^2 + (t - \mu)^2}} \exp(\delta\gamma + \beta(t - \mu)),$$

where  $K_1$  denotes a modified Bessel function of the third kind;  $\mu, \alpha, \beta$  ( $\beta < \alpha$ ) and  $\delta$  are parameters; and  $\gamma = \sqrt{\alpha^2 - \beta^2}$ . We can obtain the following moment constraints:

$$\begin{cases} \mu + \frac{\delta\beta}{\gamma} = 0 & \text{(mean)} \\ \frac{\delta\alpha^2}{\gamma^3} = 1 & \text{(variance)} \\ \frac{3\beta}{\alpha\sqrt{\delta}\gamma} = p_1 & \text{(skewness)} \end{cases}$$

Solving the constraints for mean and variance in the above equation, we can obtain  $\delta = \frac{\gamma^3}{\alpha^2}$  and  $\mu = -\frac{\delta\beta}{\gamma}$ . Hence the constraint for skewness becomes  $\frac{3\beta}{\alpha^2 - \beta^2} = p_1$ , whose solution always exists, because  $\forall p_1 \in \mathbb{R}$ , we can choose any  $\beta = \frac{p_1}{3}$  and  $\alpha = \sqrt{3\beta + p_1\beta^2}$ . Hence the attainable values of  $p_1$  are  $\mathbb{R}$ .

**Example 3.** The four-parameter Beta distribution has PDF

$$f(t; \alpha, \beta, b, c) = \frac{(t - b)^{\alpha-1}(c - t)^{\beta-1}}{(c - b)^{\alpha+\beta-1}B(\alpha, \beta)},$$

where  $\alpha > 0, \beta > 0, b, c$  ( $c > b$ ) are parameters;  $B(\alpha, \beta) = \frac{\Gamma(\alpha)\Gamma(\beta)}{\Gamma(\alpha + \beta)}$ ; and  $\Gamma$  is the Gamma function.

We can obtain the following moment constraints,

$$\begin{cases} \frac{\alpha c + \beta b}{\alpha + \beta} = 0 & \text{(mean)} \\ \frac{\alpha\beta(c-b)^2}{(\alpha+\beta)^2(\alpha+\beta+1)} = 1 & \text{(variance)} \\ \frac{2(\beta-\alpha)\sqrt{\alpha+\beta+1}}{(\alpha+\beta+2)\sqrt{\alpha\beta}} = p_1 & \text{(skewness)} \end{cases} \quad (\text{B.4})$$

Notice that if we fix any  $\beta > 0$ ,  $\frac{2(\beta-\alpha)\sqrt{\alpha+\beta+1}}{(\alpha+\beta+2)\sqrt{\alpha\beta}} \rightarrow \infty$  as  $\alpha \rightarrow 0$ ; if we fix any  $\alpha > 0$ ,  $\frac{2(\beta-\alpha)\sqrt{\alpha+\beta+1}}{(\alpha+\beta+2)\sqrt{\alpha\beta}} \rightarrow -\infty$  as  $\beta \rightarrow 0$ ; and  $\frac{2(\beta-\alpha)\sqrt{\alpha+\beta+1}}{(\alpha+\beta+2)\sqrt{\alpha\beta}} = 0$  if  $\alpha = \beta$ . Hence  $\forall p_1 \in \mathbb{R}$ , there exists  $\alpha$  and  $\beta$  such that skewness  $p_1$ . Next, we obtain the equations for  $b$  and  $c$  by solving the constraints for mean and variance in equation (B.4) as follows,

$$\begin{cases} \alpha c + \beta b = 0 \\ c - b = \frac{(\alpha+\beta)\sqrt{\alpha+\beta+1}}{\sqrt{\alpha\beta}}, \end{cases}$$

which always has a solution, because the matrix  $\begin{bmatrix} \alpha & \beta \\ 1 & -1 \end{bmatrix}$  is invertible for  $\alpha, \beta > 0$ . Hence the attainable values of  $p_1$  are  $\mathbb{R}$ .

Table 5 summarizes the results and computes attainable ranges for distributions with zero mean and unit variance:

Table 5: **Attainable Skewness for Well-Known Distributions.**

Distribution	PDF	Mean	Variance	Skewness	Attainable skewness
N $f(t; \mu, \sigma)$	$\frac{1}{\sigma\sqrt{2\pi}} e^{-\frac{1}{2}\left(\frac{t-\mu}{\sigma}\right)^2}$ ( $\mu \in \mathbb{R}, \sigma > 0$ )	$\mu$	$\sigma^2$	0	0
T $f(t; \mu, \sigma, \nu)$	$\frac{\Gamma\left(\frac{\nu+1}{2}\right)}{\Gamma\left(\frac{\nu}{2}\right)\sqrt{\pi\nu}\sigma} \left(1 + \frac{1}{\nu}\left(\frac{t-\mu}{\sigma}\right)^2\right)^{-\frac{\nu+1}{2}}$ ( $\mu \in \mathbb{R}, \nu, \sigma > 0$ )	$\mu$	$\frac{\nu}{\nu-2}\sigma^2$	0	0
SN $f(t; \xi, \omega, \alpha)$	$\frac{2}{\Omega n} \phi\left(\frac{t-\xi}{\Omega n}\right) \Phi\left(\alpha\left(\frac{t-\xi}{\Omega n}\right)\right)$ ( $\xi, \alpha \in \mathbb{R}, \omega > 0, \delta = \alpha/\sqrt{1+\alpha^2}$ )	$\xi + \omega\delta\sqrt{\frac{2}{\pi}}$	$\omega^2\left(1 - \frac{2\delta^2}{\pi}\right)$	$\frac{\sqrt{2}(4-\pi)\delta^3}{(\pi-2\delta^2)^{3/2}}$	$(-0.995, 0.995)$
NIG $f(t; \alpha, \beta, \delta, \mu)$	$\frac{\alpha\delta K_1\left(\alpha\sqrt{\delta^2+(t-\mu)^2}\right)}{\pi\sqrt{\delta^2+(t-\mu)^2}} e^{\delta\gamma+\beta(t-\mu)}$ ( $\alpha, \beta, \delta, \mu \in \mathbb{R},  \alpha  \geq  \beta $ )	$\mu + \frac{\delta\beta}{\gamma^3}$	$\frac{\delta\alpha^2}{\gamma^3}$	$\frac{3\beta}{\alpha\sqrt{\delta}\gamma}$	$\mathbb{R}$
Beta $f(t; \alpha, \beta, b, c)$	$\frac{(t-b)^{\alpha-1}(c-t)^{\beta-1}}{(c-b)^{\alpha+\beta-1}B(\alpha,\beta)}$ ( $\alpha, \beta, b, c \in \mathbb{R}, c > b$ )	$\frac{\alpha c + \beta b}{\alpha + \beta}$	$\frac{\alpha\beta(c-b)^2}{(\alpha+\beta)^2(\alpha+\beta+1)}$	$\frac{2(\beta-\alpha)\sqrt{\alpha+\beta+1}}{(\alpha+\beta+2)\sqrt{\alpha\beta}} \in \mathbb{R}$	$\mathbb{R}$